

## Metallogenic Mechanism and Tectonic Setting of Tungsten Mineralization in the Yangbishan Deposit in Northeastern China

HAO Yujie<sup>1,2</sup>, REN Yunsheng<sup>1,2,\*</sup>, ZHAO Hualei<sup>3</sup>, LAI Ke<sup>1</sup>, ZHAO Xuan<sup>1</sup> and MA Yupeng<sup>1</sup>

1 College of Earth Sciences, Jilin University, Changchun 130061, Jilin, China

2 Key Laboratory of Mineral Resources Evaluation in Northeast Asia, Ministry of Land and Resources of China, Changchun 130026, Jilin, China

3 Tianjin Institute of Geology and Mineral Resources, Tianjin 300170, China

**Abstract:** The Yangbishan iron–tungsten deposit in the Shuangyashan area of Heilongjiang Province is located in the center of the Jiamusi Massif in northeastern China. The rare earth element and trace element compositions of the scheelite show that it formed in a reducing environment and inherited the rare earth element features of the ore-forming fluid. The geochemical characteristics of the gneissic granite associated with the tungsten mineralization show that the magma formed in this reducing environment and originated from the partial melting of metamorphosed shale that contained organic carbon and was enriched with tungsten. In addition, in situ Hf isotopic analysis of zircons from the gneissic granite indicates that they probably originated from the partial melting of a predominantly Paleo–Mesoproterozoic crustal source. According to LA-ICP-MS zircon dating, the Yangbishan ore-related gneissic granite has an Early Paleozoic crystallization age of  $520.6 \pm 2.8$  Ma. This study, together with previous data, indicates that the massifs of northeastern China, including Erguna, Xing'an, Songliao, Jiamusi, and Khanka massifs, belonged to an orogenic belt that existed along the southern margin of the Siberian Craton during the late Pan-African period. The significant continental movements of this orogeny resulted in widespread magmatic activity in northeastern China from 530 Ma to 470 Ma under a tectonic setting that transitioned from compressional syn-collision to extensional post-collision.

**Key word:** scheelite, Yangbishan iron–tungsten deposit, Early Paleozoic, late Pan-African period, Central Asian Orogenic Belt

### 1 Introduction

In past twenty years, more than ten tungsten deposits have been found in northeast China, north of the Xilamulun–Changchun suture, including three large- and six medium-sized deposits. The deposits at Yangjingou, Honghuaerji, Wudaogou, and Shamai can be classified as lode-type (Ren Yunsheng et al., 2010a, 2011; Guo et al., 2016; Jiang et al., 2016), and polymetallic tungsten deposits at Cuihongshan, Yangbishan, Baishilazi, Sanjiazi, and Gongpengzi are skarn-type (Ren Yunsheng et al., 2010b; Zhao Hualei et al., 2011; Hao Yujie et al., 2013; Liu Yu, 2013; Zhao Hualei, 2014). There is clearly great potential for further discoveries of tungsten deposits in the region.

In recent years, the tungsten deposits in NE China have

garnered increasing attention from researchers, who have discussed the geological conditions of ore formation, the ore genesis, the characteristics of the ore-forming fluid, the mineralization age, and the tectonic setting (Ren Yunsheng et al., 2010a, b, 2011; Hao Yujie et al., 2013; Liu Yu, 2013; Ouyang et al., 2013; Mao et al., 2014; Zhao Hualei, 2014; Liu et al., 2015; Guo et al., 2016; Jiang et al., 2016). With the exception of several late Paleozoic deposits, such as the Wudaogou and Yangjingou deposits (Zhao Hualei, 2014), the data suggest that the tungsten deposits in northeast China formed during the Mesozoic. While the Yangbishan iron–tungsten deposit, discovered six decades ago, has received little attention, and the research has focused mainly on the local iron mineralization (Tan Chengyin, 2009; Wei Lianxi, 2013). The tectonic setting, age, and mechanism of tungsten mineralization in this deposit are unknown. To provide

\* Corresponding author. E-mail: renys@jlu.edu.cn

this information, we carried out a field investigation of the Yangbishan deposit and conducted laser ablation inductively coupled plasma mass spectrometry (LA-ICP-MS) zircon U–Pb dating, zircon Hf isotope analyses, major and trace element analysis of the gneissic granite, and trace and rare element analysis of the scheelite.

## 2 Regional Geological Background

The Yangbishan iron–tungsten deposit in the Shuangyashan area of Heilongjiang Province is located in the eastern part of the Central Asian Orogenic Belt (CAOB) and is in the middle of the Jiamusi Massif (Zhao Liangliang et al., 2014) (Fig. 1a). The study area develops the metamorphosed basement with the sedimentary cover. The basement, from the bottom to top, consists of the Paleoproterozoic–Archean Mashan Group, the Mesoproterozoic Xingdong Group, the Neoproterozoic Heilongjiang Group, and the Sinian Majiajie Group (Heilongjiang Bureau of Geology and Mineral Resources (HBGMR), 1993). The Mashan and Xingdong groups are primarily distributed within the Jiamusi Massif, the Heilongjiang Group is distributed in the west and along the southern margin of the Massif, and the Majiajie Group is located only in the southern Huanan area. The sedimentary

cover includes Paleozoic, Mesozoic, and Cenozoic strata, and occurs mainly in the northern part of the Jiamusi Massif (Fig. 1b).

The Jiamusi Massif experienced the formation of an ancient Archean continental nucleus, the formation and evolution of Proterozoic rifts and fault depressions, early Paleozoic cratonization, the late Paleozoic closure of the Paleo-Asian Ocean, and the Mesozoic subduction of the Paleo-Pacific Plate (Zhao Liangliang et al., 2014). The Paleozoic tectonic activity is represented by folds in the metamorphic basement, while the Mesozoic tectonic activity left brittle, deep faulting that created the basic structural pattern of the Jiamusi Massif. These faults include the Mudanjiang Fault in the west, the Dunhua–Mishan Fault in the south, and the Tongjiang–Dangbi Fault in the east (Fig. 1a and b).

In addition, there is evidence of three stages of magmatism that occurred during the early Paleozoic, late Paleozoic, and Mesozoic. The early Paleozoic intrusions, which occur mainly in the Jiamusi–Baoqing–Jixi area, were emplaced between 480 and 530 Ma (Wilde et al., 2001, 2003; Xie Hangqiang et al., 2008). Late Paleozoic intrusions, with ages from 280 to 250 Ma, are widespread in Jiamusi Massif (Huang Yingcong et al., 2009). A series of Mesozoic basic, moderate and acidic magmatic rocks

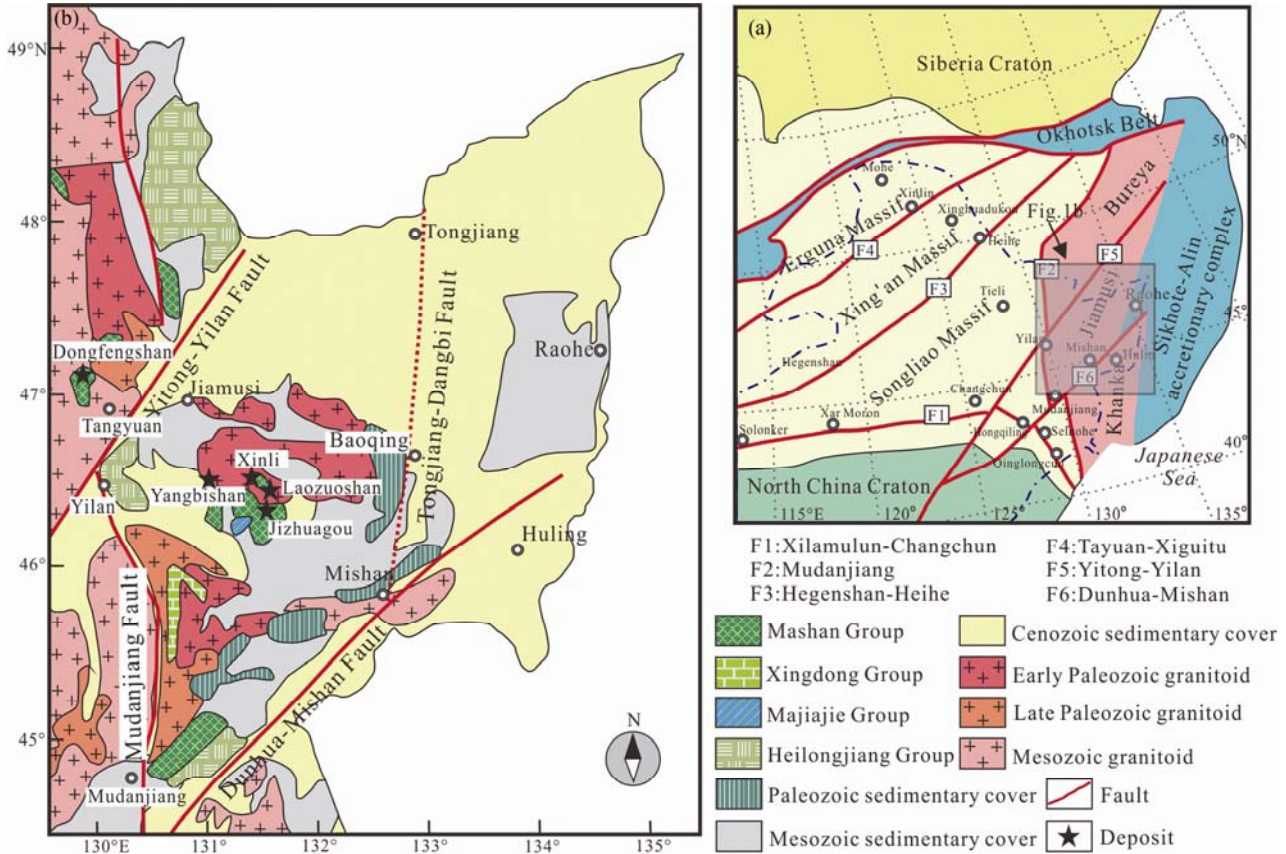


Fig. 1. Sketch tectonic map (a) (after Ge Wenchun et al., 2007b) and simplified geological map (b) (after Wilde et al., 2000) of the Jiamusi Massif.

are closely associated with mineralization of precious and non-ferrous metals. The Mesozoic was the most important mineralization period in the eastern part of Heilongjiang Province (Li Yixin, 2012).

### 3 Ore Deposit Geology and Tungsten Mineralization

#### 3.1 Ore deposit geology

The Mesoproterozoic Dapandao Formation of the

Xingdong Group ( $Pt_2dp$ ) (Fig. 2a and b), which is closely associated with the iron–tungsten mineralization in the Yangbishan mining area, can be divided into four lithologic units. From bottom to top, the first lithologic unit is mainly composed of garnet–mica–quartz schist, sillimanite–garnet–plagioclase schist, and gneiss, with some interspersed magnetite quartzites; the second unit comprises marble and schist that host crystalline graphite ore; the third unit is mainly composed of gneiss and sillimanite–biotite–quartz schist with layers of magnetite

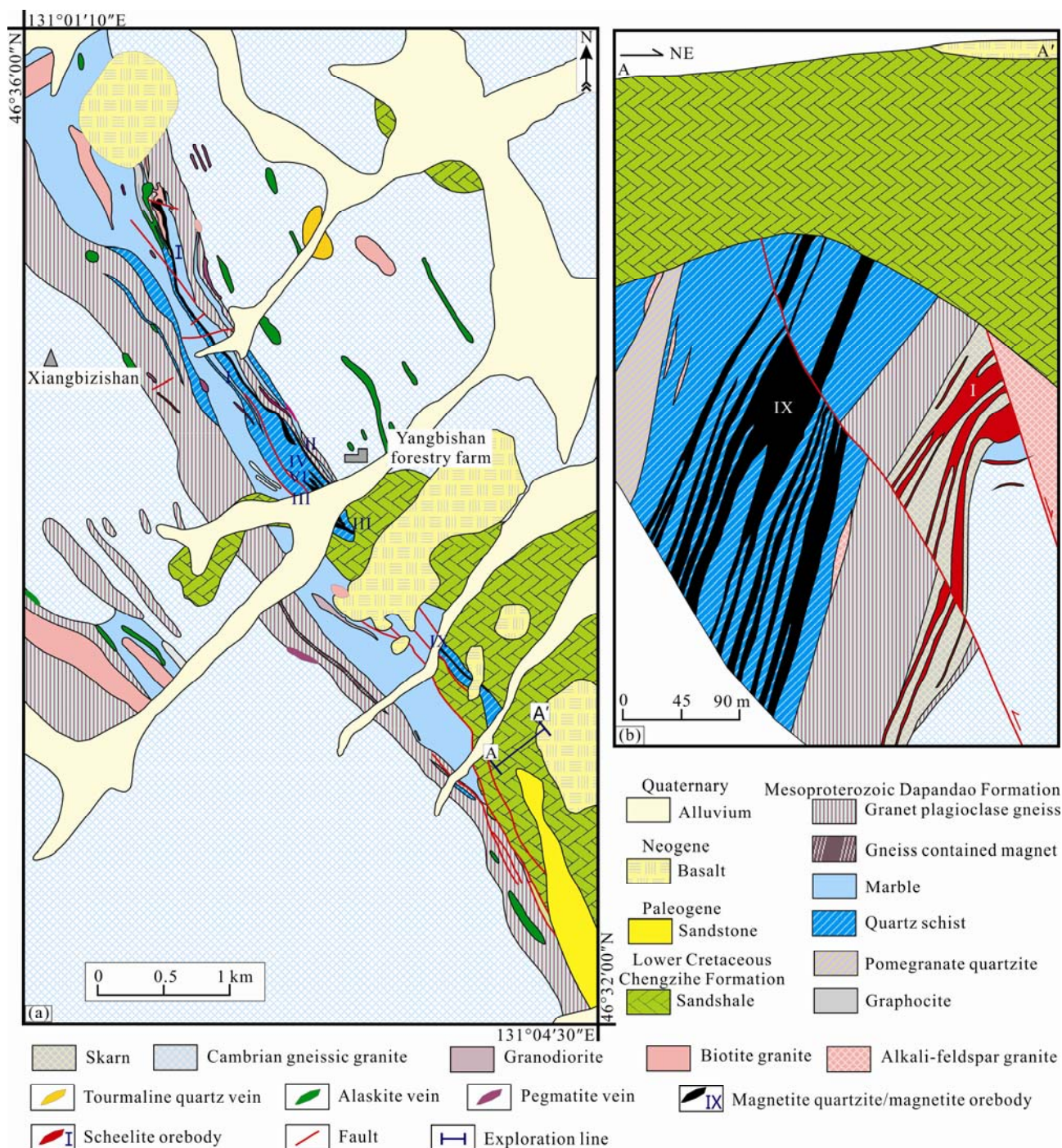


Fig. 2. Sketch geological map (a) and cross section of the Yangbishan deposit (b) (modified from Tan Chengyin, 2009).

ore; and the fourth unit is composed of schist, gneiss, and marble.

The widespread magmatic rocks associated with the Yangbishan deposit are mainly gneissic granite, exposed sporadically among the rocks of the ore-hosting Dapandao Formation of the Xingdong Group. These granitic rocks underwent ductile deformation, leading to their weak gneissic structures, and consist mainly of K-feldspar (~30% by volume), plagioclase (~20%), biotite (~15%), muscovite (~5%), and quartz (~30%). In addition, there is a small, late-stage biotite granite stock that intruded into the gneissic granite. Small amounts of leucogranite and pegmatite veins also occur in the area.

The structures in the mining area mainly include small-scale faults, fractures, and interlayer fracture zones. These faults and fractures can be divided into three groups according to their orientations: NE–SW, E–W, and SE–NW. The largest group of faults runs NE–SW, which formed in association with the later-stage activities of the Paleo-Pacific tectonic domain. Although in small-scale, the roughly E–W-trending faults have had the most disruptive effect on the ore bodies. Locally, the Dapandao Formation strata have been cut by NE–SW and NW–SE reverse faults, resulting in the formation of small, overturned anticlines and synclines that trend more or less E–W and pitch to the west.

### 3.2 Tungsten mineralization

Six buried tungsten ore bodies (I–VI) were explored in the footwall rock of the iron ore bodies in the southern part of the mining area (Fig. 2a and b). They are situated in the contact zone between the gneissic granite (Fig. 2a) and the marble of the Dapandao Formation (Fig. 2b). The largest body, ore body I, is 1,040 m long and 11.6 m thick, on average, and it extends down 305 m as lense and vein. Locally, the thickness of the ore body increases dramatically, reaching a maximum thickness of 88 m. The ore body dips 60–80° toward 210–250°. The average ore grade of WO<sub>3</sub> is 0.38%, peaking at 2.75%. The roof wall rocks of the ore body are marble (Fig. 3a) and skarn, and foot wall rocks include gneissic granite (Fig. 3b and c) and skarn.

Ore-bearing rocks of tungsten mineralization in the Yangbishan deposit include garnet skarn and diopside skarn. Metallic minerals in the tungsten ores are dominated by scheelite and pyrrhotite (Fig. 3d–e), with small amounts of magnetite, pyrite, chalcopyrite, sphalerite, cassiterite, arsenopyrite and molybdenite (Fig. 3d–k). The major nonmetallic minerals include augite, quartz, calcite, and diopside (Fig. 3k–o), with smaller amounts of plagioclase, garnet, chlorite, epidote, potassium feldspar, idocrase, tourmaline, and fluorite (Fig. 3l). Metallic minerals in the ore are often characterized by

xenomorphic or subidiomorphic granular textures (Fig. 3f, g, k), followed by automorphic granular, metasomatic relict (Fig. 3h) and intersertal textures. The ore structures are mainly disseminated, densely disseminated, or vein structures (Fig. 3e).

The major wall-rock alteration types include skarnization, silicification, carbonatation, chloritization, epidotization, and fluoritization (Fig. 3k–o), with skarnization being the most common and widespread. The pattern of alteration weakens from the center of the contact zone to the gneissic granite and the marble, but it produced a local abundance of skarn.

According to the mineral assemblages, ore textures and structures, and wall-rock alteration, the tungsten mineralization in the Yangbishan deposit formed in two periods, the skarn period and the quartz–sulfide period, which comprise five stages (Fig. 4). The oxide stage of the skarn period was the major tungsten mineralization stage.

## 4 Samples and Analytical Methods

### 4.1 LA-ICP-MS zircon U–Pb dating

One gneissic granite sample (No. YBS4–1) for LA-ICP-MS zircon U–Pb dating was collected nearby the tungsten ore body I in the open pit in the south segment of the Yangbishan deposit (geographic coordinates of slope collar, N46°33'37", E131°03'47"). Zircon grains were separated by heavy liquid and magnetic separation methods at the Chengxin Services Ltd., Langfang, China. Pure zircon grains were handpicked under a binocular microscope, then mounted in epoxy resin and polished until the grain interiors were exposed. The Cathodoluminescence (CL) images were obtained using a JSM6510 scanning electron microscope produced by JEOL Corporation (Japan) at the Beijing zircon dating navigation technology limited company. LA-ICP-MS U–Pb zircon dating was carried out at the Key Laboratory of Mineral Resources Evaluation in Northeast Asia, Ministry of Land and Resources, Jilin University, Changchun, China. Helium was used as carrier gas to provide efficient aerosol transport to the ICP and minimize aerosol deposition around the ablation site and within the transport tube (Eggins et al., 1998; Jackson et al., 2004). Argon was used as the make-up gas and was mixed with the carrier gas via a T–connector before entering the ICP. The analysis spots were 25 μm in diameter. U, Th and Pb concentrations were calibrated using <sup>29</sup>Si as an internal standard. The standard zircon 91500 (Wiedenbeck et al., 1995) was used as an external standard to normalize isotopic fractionation during analysis. Analytical procedures used follow those described by Yuan et al., (2007). Raw data were processed using the

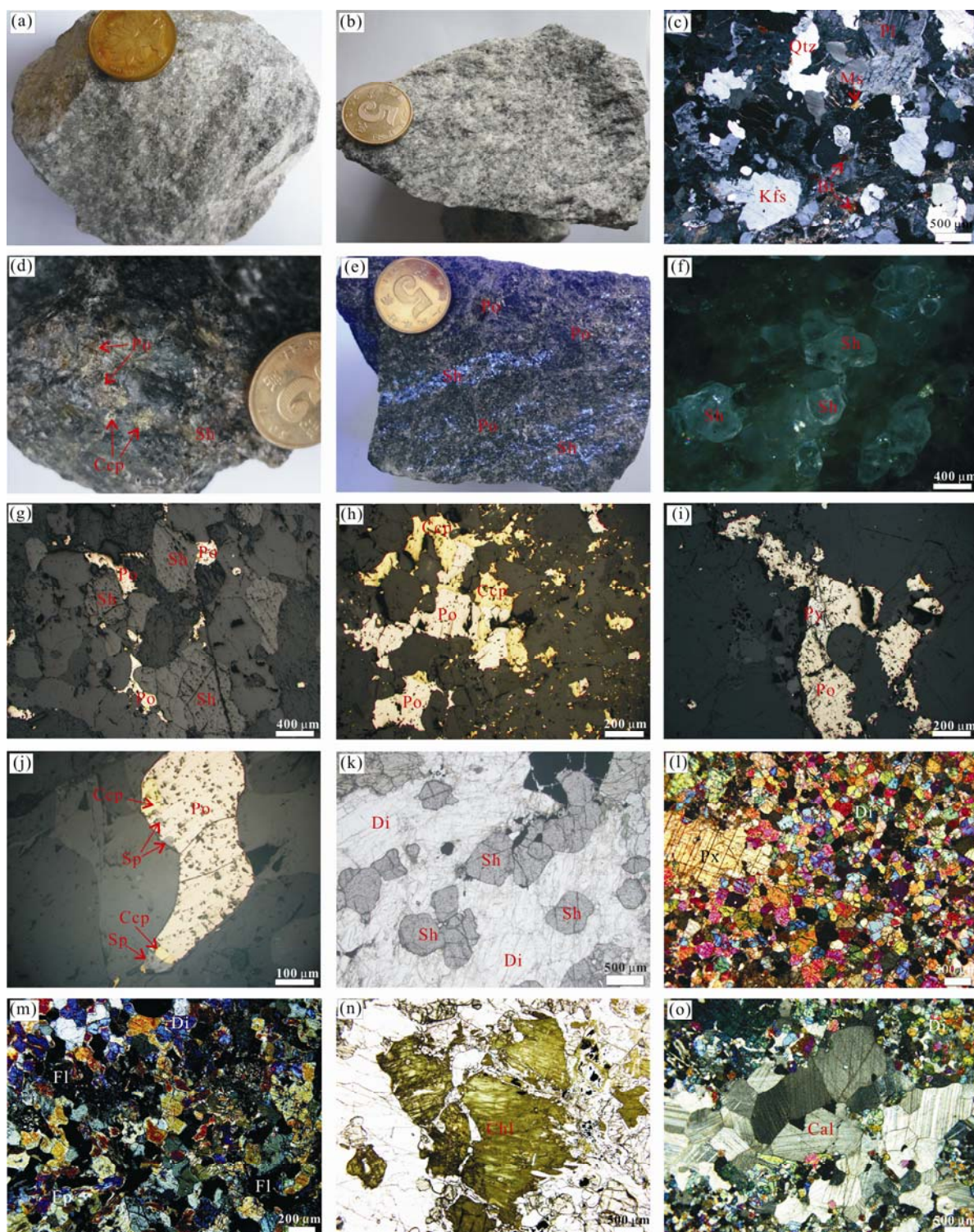


Fig. 3. Characteristics of the mineralization-related rock body and tungsten ore in the Yangbishan deposit.

(a), Hand specimen of marble; (b), Hand specimen of gneissic granite; (c), Diopside marble; (d), Scheelite coexisting with pyrrhotite and chalcopyrite; (e), Disseminated and vein scheelite in diopside skarn; (f), Internal reflection of scheelite; (g), Scheelite being replaced by pyrrhotite; (h), Chalcopyrite being replaced by pyrrhotite; (i), Pyrrhotite being replaced by pyrite; (j), Pyrrhotite being replaced by chalcopyrite and sphalerite; (k), Diopside encapsulated scheelite; (l), Diopside skarn; (m), Fluoritization in epidote diopside skarn; (n), Chloritization in skarn; (o), Carbonatation in epidote skarn. Abbreviations: Bt, biotite; Cal, calcite; Ccp, chalcopyrite; Di, diopside; Ep, epidote; Fl, fluorite; Kfs, potassium feldspar; Mag, magnetite; Ms, muscovite; Pl, plagioclase; Po, pyrrhotite; Px, augite; Py, pyrite; Qtz, quartz; Sh, scheelite; Sp, sphalerite. Photos g, h, i, j, k and n are taken under single polarizer, and photos b, f, c, m and o are taken under crossed nicols.

Metallogenic stages Minerals	Skarn period			Quartz-sulfide period	
	Early skarn stage	Late skarn stage	Oxide stage	Early quartz-sulfide stage	Late quartz-sulfide stage
Grossularite	██████████	██████████			
Diopside	██████████	██████████	██████████		
Augite	██████████				
Tremolite	██████████	██████████	██████████		
Hornblende		██████████			
Actinolite		██████████			
Plagioclase	██████████	██████████	██████████		
Epidote		██████████	██████████		
Quartz			██████████	██████████	██████████
Muscovite			██████████		
Chlorite				██████████	
Magnetite		██████████	██████████		
Scheelite			██████████	██████████	
Pyrite				██████████	██████████
Pyrrhotite				██████████	██████████
Chalcopyrite				██████████	██████████
Sphalerite				██████████	██████████
Calcite					██████████

Fig. 4. Paragenetic sequence of minerals in tungsten ore from the Yangbishan deposit.

ICPMSDataCal program (Version 6.7) (Liu et al., 2008). Uncertainties of individual analyses are reported with  $1\sigma$  error; weighted mean ages were calculated at  $1\sigma$  confidence level. The data were processed using the ISOPLOT (Version 3.0) program (Ludwig, 2003). The zircon GJ-1 was dated as an unknown sample and yielded a weighted mean  $^{206}\text{Pb}/^{238}\text{U}$  age of  $609.5 \pm 2.4$  Ma ( $n=8$ ,  $2\sigma$ ), which is in good agreement with the recommended age of  $608.5 \pm 0.37$  Ma (Simon et al., 2004).

#### 4.2 Major and trace element analyses of gneissic granite

Five gneissic granite samples (No. Y1-1 to Y1-5) for geochemical analyses were collected from the tunnel in the mine area. All samples are fresh and without obvious alteration. Major and trace element analyses were obtained at the Laboratory of Mineralization and Dynamics, Chang'an University, Xi'an, China. Major elements were assayed by X-ray fluorescence (XRF) and trace elements and rare earth elements were assayed by Thermo-X7 ICP-MS. Parameters of the analysis were: Power: 1200 W, Nebulizer gas: 0.64 L/min, Auxiliary gas: 0.80 L/min and Plasma gas: 13 L/min.

#### 4.3 Zircon Hf isotope analyses of gneissic granite

Zircon Hf isotope analyses were conducted in situ using a New Wave UP213 laser-ablation microprobe attached to a Neptune multi-collector ICP-MS at the Institute of Mineral Resources, Chinese Academy of Geological

Sciences, Beijing. The instrumental conditions and data acquisition follow those described by Hou Kejun et al., (2007). A stationary spot with a beam diameter of either 40  $\mu\text{m}$  or 55  $\mu\text{m}$  was used, depending on the size of the ablated domains, He gas, in combination with Ar, was used as the carrier gas to transport the ablated sample from the laser-ablation cell to the ICP-MS torch via a mixing chamber. To correct for the isobaric interferences of  $^{176}\text{Lu}$  and  $^{176}\text{Yb}$  with  $^{176}\text{Hf}$ ,  $^{176}\text{Lu}/^{175}\text{Lu} = 0.02658$  and  $^{176}\text{Yb}/^{173}\text{Yb} = 0.796218$  ratios were determined (Chu et al., 2002). For instrumental mass bias corrections, Yb isotope ratios were normalized to a  $^{172}\text{Yb}/^{173}\text{Yb}$  ratio of 1.35274 (Chu et al., 2002) and Hf isotope ratios to a  $^{179}\text{Hf}/^{177}\text{Hf}$  ratio of 0.7325 using an exponential law. The mass bias behavior of Lu was assumed to follow that of Yb. The mass bias correction protocols were performed as described by Hou Kejun et al., (2007). Zircon GJ1 was used as a standard reference material during routine analyses; its weighted mean  $^{176}\text{Hf}/^{177}\text{Hf}$  ratio of  $0.282008 \pm 27$  ( $2\sigma$ ) is indistinguishable from that obtained in the in situ analysis conducted by Elhlou et al., (2006) ( $^{176}\text{Hf}/^{177}\text{Hf} = 0.282014 \pm 20$ ;  $2\sigma$ ).

The calculation of the Hf model age (single-stage model age;  $T_{\text{DM1}}$ ) is based on a depleted-mantle source with a modern  $^{176}\text{Hf}/^{177}\text{Hf}$  ratio of 0.28325 and the  $^{176}\text{Lu}$  decay constant  $1.865 \times 10^{-11} \text{ year}^{-1}$  (Scherer et al., 2001). The calculation of the "crust" (two-stage) Hf model age ( $T_{\text{DM2}}$ ) is based on the assumption of a mean  $^{176}\text{Lu}/^{177}\text{Hf}$

value of 0.011 for average continental crust (Wedepohl, 1995). The calculation of  $\epsilon_{\text{Hf}}(t)$  values was based on zircon U–Pb ages and chondritic values ( $^{176}\text{Hf}/^{177}\text{Hf} = 0.282772$ ,  $^{176}\text{Lu}/^{177}\text{Hf} = 0.0332$ ; Blichert-Toft and Albarede, 1997).

#### 4.4 Rare earth and trace element analyses of the scheelite

Scheelite samples in this study were collected from the tungsten ore bodies in the Yangbishan deposit. Rare earth element analyses (samples YBS01, YBS1–3, YBS42–1, YBS42–2, and YBS42–3) were completed at the State Key Laboratory for Mineral Deposits Research, Nanjing University. Rare earth and trace element analyses (samples YB–11–1, YB–11–2, YB–8, Y1–6, and Y1–4) were completed in the Analytical Laboratory of the Beijing Research Institute of Uranium Geology. Analytical instruments and procedures used follow those described by Ren Yunsheng et al. (2010a).

## 5 Results

### 5.1 LA-ICP-MS zircon dating

The LA-ICP-MS zircon U–Pb dating results of the gneissic granite closely related to the tungsten mineralization are listed in Table 1.

According to shapes, growth zoning in CL images, contents and ratio values of Th and U, zircon grains can be divided into three groups (Fig. 5). Zircon grains in the group one are granular and round, with lengths between 60 to 120  $\mu\text{m}$ , lower contents of Th and U, brighter CL images and clear oscillatory zoning (e.g. YBS4–1–18 and YBS4–1–42). The Th/U ratios of nine zircons are between 0.03 and 0.85 with average 0.27, indicating magmatic origin of these grains (Song Biao et al., 2002; Corfu et al., 2003; Samuel and Mark, 2003); the  $^{207}\text{Pb}/^{206}\text{Pb}$  ages of this group are scattered, and between  $1150 \pm 26$  Ma and  $1812 \pm 34$  Ma (Table 1 and Fig. 6a). Zircon grains of group two have good crystal shape with short plate and long column, and the average ratio of length to width is 3:1 (a total of 31 dating

**Table 1 LA-ICP-MS zircon U–Pb dating results of grains from the Yangbishan gneissic granite**

Sample No.	Concentration(ppm)		Ratio						Age(Ma)			
	Th	U	Th/U	$^{207}\text{Pb}/^{206}\text{Pb}$	$1\sigma$	$^{207}\text{Pb}/^{235}\text{U}$	$1\sigma$	$^{206}\text{Pb}/^{238}\text{U}$	$1\sigma$	$^{207}\text{Pb}/^{206}\text{Pb}$	$^{207}\text{Pb}/^{235}\text{U}$	$^{206}\text{Pb}/^{238}\text{U}$
YBS4-1-1	6715	10503	0.64	0.0634	0.0015	0.2527	0.0064	0.0288	0.0004	730±30	229±5	183±2
YBS4-1-2	1178	4062	0.29	0.0619	0.0011	0.7218	0.0148	0.0842	0.0011	700±18	552±9	521±7
YBS4-1-3	472	2815	0.17	0.0642	0.0013	0.7478	0.0141	0.0844	0.0011	762±19	567±8	523±6
YBS4-1-4	310	3709	0.08	0.0609	0.0013	0.6839	0.0153	0.0808	0.0007	588±23	529±9	501±4
YBS4-1-5	372	1121	0.33	0.0571	0.0013	0.6682	0.0156	0.0845	0.0009	521±31	520±10	523±5
YBS4-1-6	399	6239	0.06	0.0663	0.0017	0.7722	0.0203	0.0842	0.0013	857±26	581±12	521±7
YBS4-1-7	143	2451	0.06	0.0598	0.0012	0.7013	0.0145	0.0844	0.0007	639±28	540±9	522±4
YBS4-1-8	353	1937	0.18	0.0700	0.0015	0.8207	0.0182	0.0844	0.0008	919±27	608±10	522±5
YBS4-1-9	577	1495	0.39	0.0604	0.0013	0.7038	0.0141	0.0843	0.0008	594±26	541±8	522±4
YBS4-1-10	406	3250	0.12	0.0622	0.0012	0.7289	0.0153	0.0844	0.0007	662±24	556±9	522±4
YBS4-1-11	296	2270	0.13	0.0624	0.0015	0.7293	0.0175	0.0843	0.0010	673±27	556±10	522±6
YBS4-1-12	185	827	0.22	0.0791	0.0018	2.2485	0.0498	0.2051	0.0019	1150±26	1196±16	1202±10
YBS4-1-13	826	1618	0.51	0.0612	0.0015	0.7154	0.0184	0.0843	0.0008	626±32	548±11	522±5
YBS4-1-14	919	3096	0.30	0.0883	0.0015	2.5163	0.0490	0.2056	0.0024	1409±18	1277±14	1205±13
YBS4-1-15	726	8716	0.08	0.0585	0.0010	0.4269	0.0084	0.0527	0.0005	554±24	361±6	331±3
YBS4-1-16	101	333	0.30	0.0906	0.0022	2.8025	0.0668	0.2243	0.0027	1423±20	1356±18	1304±14
YBS4-1-17	686	2349	0.29	0.0577	0.0010	0.6744	0.0135	0.0844	0.0007	487±26	523±8	522±4
YBS4-1-18	160	410	0.39	0.0841	0.0022	2.5857	0.0734	0.2231	0.0032	1240±28	1297±21	1298±17
YBS4-1-19	584	1811	0.32	0.0568	0.0012	0.6632	0.0151	0.0844	0.0008	467±28	517±9	522±5
YBS4-1-20	102	284	0.36	0.0819	0.0022	2.3081	0.0576	0.2048	0.0020	1255±32	1215±18	1201±11
YBS4-1-21	273	2240	0.12	0.0592	0.0012	0.6908	0.0137	0.0843	0.0009	543±23	533±8	522±5
YBS4-1-22	478	673	0.71	0.0795	0.0015	2.4659	0.0450	0.2236	0.0019	1203±20	1262±13	1301±10
YBS4-1-23	29	979	0.03	0.0587	0.0016	0.6865	0.0176	0.0849	0.0016	555±27	531±11	525±10
YBS4-1-24	122	541	0.22	0.0662	0.0020	0.7734	0.0224	0.0847	0.0016	812±31	582±13	524±10
YBS4-1-25	32	64	0.50	0.1108	0.0040	3.8436	0.1332	0.2516	0.0053	1812±34	1602±28	1447±27
YBS4-1-26	167	563	0.30	0.0579	0.0023	0.6846	0.0256	0.0857	0.0017	527±48	530±15	530±10
YBS4-1-27	111	671	0.16	0.0575	0.0017	0.6481	0.0180	0.0817	0.0016	512±30	507±11	506±9
YBS4-1-28	549	980	0.56	0.0586	0.0016	0.7050	0.0184	0.0873	0.0017	552±27	542±11	539±10
YBS4-1-29	227	507	0.45	0.0578	0.0023	0.6645	0.0254	0.0834	0.0017	522±49	517±16	516±10
YBS4-1-30	247	1073	0.23	0.0577	0.0015	0.6735	0.0166	0.0847	0.0016	518±25	523±10	524±9
YBS4-1-31	237	309	0.77	0.0934	0.0026	3.3449	0.0887	0.2596	0.0051	1497±24	1492±21	1488±26
YBS4-1-32	122	491	0.25	0.0588	0.0018	0.6887	0.0202	0.0849	0.0016	561±33	532±12	525±10
YBS4-1-33	119	285	0.42	0.0579	0.0026	0.6680	0.0288	0.0837	0.0017	524±59	520±18	518±10
YBS4-1-34	178	1075	0.17	0.0585	0.0018	0.6719	0.0192	0.0834	0.0016	547±31	522±12	516±10
YBS4-1-35	47	873	0.05	0.0589	0.0017	0.6886	0.0191	0.0847	0.0016	565±30	532±12	524±10
YBS4-1-36	86	524	0.16	0.0580	0.0019	0.6767	0.0213	0.0846	0.0017	530±37	525±13	524±10
YBS4-1-37	126	439	0.29	0.0583	0.0019	0.7024	0.0225	0.0873	0.0017	543±37	540±13	540±10
YBS4-1-38	351	655	0.54	0.0578	0.0020	0.6818	0.0229	0.0856	0.0017	522±40	528±14	529±10
YBS4-1-39	465	548	0.85	0.0576	0.0021	0.6489	0.0226	0.0817	0.0016	514±43	508±14	506±10
YBS4-1-40	183	362	0.51	0.0582	0.0024	0.6787	0.0274	0.0845	0.0017	538±53	526±17	523±10
YBS4-1-41	102	572	0.18	0.0618	0.0024	0.7392	0.0272	0.0867	0.0018	668±45	562±16	536±10
YBS4-1-42	228	225	1.02	0.1074	0.0029	4.6148	0.1178	0.3116	0.0062	1756±22	1752±21	1748±30

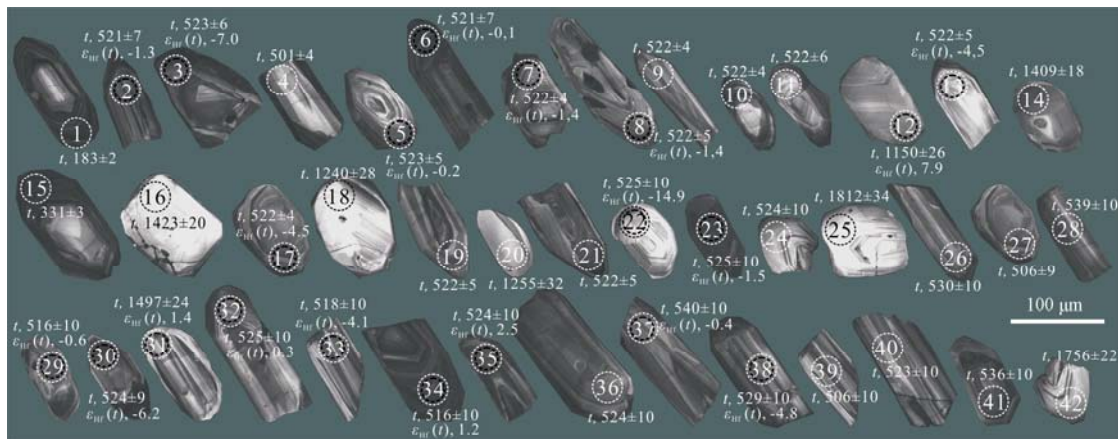


Fig. 5. CL images and dating spots of zircons from the Yangbishan gneissic granite.

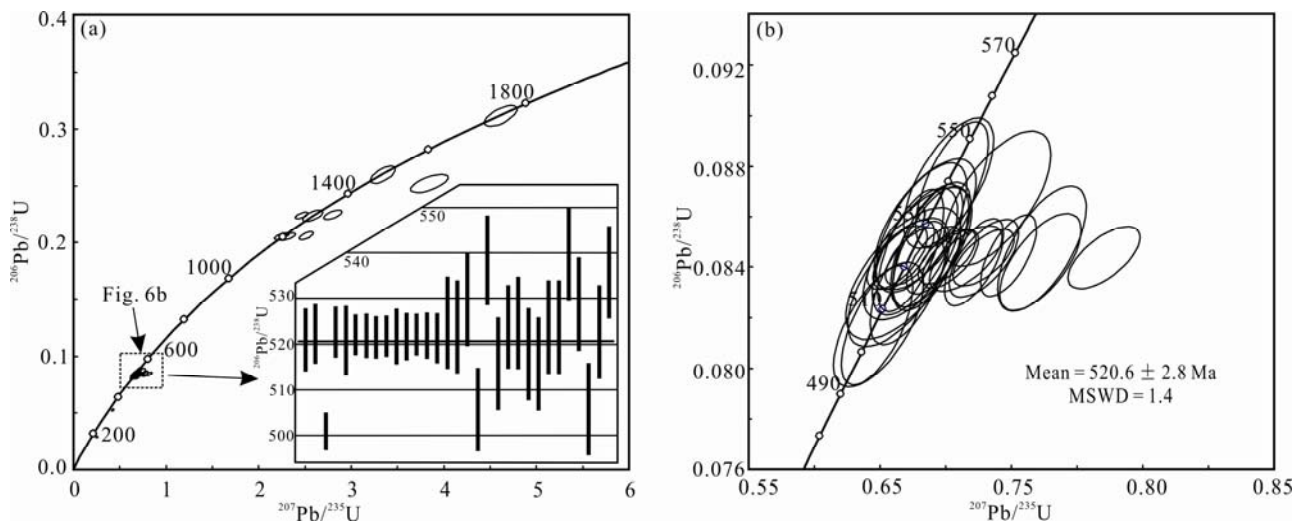


Fig. 6. Concordia and weighted diagrams of the zircon U–Pb age of the gneissic granite from the Yangbishan deposit.

spots, e.g. YBS4–1–26 and YBS4–1–38). The particle sizes are from 60 to 200  $\mu\text{m}$  with higher Th and U contents, and the Th/U ratios are between 0.12 and 0.56 with average 0.27. Zircon grains in this group have clear oscillatory zoning, indicating their magmatic origin. The  $^{206}\text{Pb}/^{238}\text{U}$  ages of 31 zircons range from  $501 \pm 4$  Ma to  $540 \pm 10$  Ma, with a weighted average age of  $520.6 \pm 2.8$  Ma (MSWD = 1.4) (Fig. 6b and c). Zircon grains in group three have perfect crystal shape as long column with obvious oscillatory zoning, but the two dating ages deviated concordia line obviously, which is probably related to the Pb lose by the late thermal disturbance. Thus, this group has not been discussed (Fig. 6a).

## 5.2 Major and trace elements in gneissic granite

Major element compositions of the Yangbishan gneissic granite are listed in Table 2. The gneissic granite is characterized by high silica ( $\text{SiO}_2 = 71.28\text{--}72.84$  wt%), and rich in alkali ( $\text{Na}_2\text{O} + \text{K}_2\text{O} = 7.57\text{--}8.31$  wt%). In these samples,  $\text{K}_2\text{O}$  contents are 4.58–5.10 wt%,  $\text{Na}_2\text{O}$  contents are 2.64–3.25 wt%, and  $\text{Na}_2\text{O}/\text{K}_2\text{O}$  ratios are from 0.52 to

0.67, which indicates that these samples are relatively rich in potassium. In addition, these samples are characterized by lower contents of  $\text{Fe}_2\text{O}_3^{\text{T}}$ ,  $\text{MgO}$ ,  $\text{MnO}$ ,  $\text{CaO}$ , and  $\text{P}_2\text{O}_5$ . A/CNK is 1.12–1.25. Their Rittmann index ( $\delta$ ) ranges from 1.96 to 2.79. Their differentiation index (DI) ranges from 89 to 90, indicating that the gneissic granite may be derived from highly fractionated magma. In the QAP classification diagram (Fig. 7a), these sample polts fall in the region of granite. In the A/NK–A/CNK diagram (Fig. 7b), these sample plots fall in the region of peraluminous rock.

Rare earth and trace element compositions of the Yangbishan gneissic granite are listed in Table 2. The total rare earth element (REE) contents of the samples range from 87.12 ppm to 122.12 ppm (mean 106.11 ppm), while light rare earth elements (LREEs) are relatively enriched (LREE/HREE = 7.51–11.15). Fractionation of LREEs and HREEs is clear [ $(\text{La}/\text{Yb})_{\text{N}} = 9.53\text{--}20.26$ ]. All samples display an obvious Eu negative anomaly ( $\delta\text{Eu} = 0.40\text{--}0.69$ ), and cerium displays a slightly negative Ce anomaly ( $\delta\text{Ce} = 0.87\text{--}0.97$ ). In chondrite-normalized REE diagram

**Table 2 Major and trace element compositions of the Yangbishan gneissic granite**

Sample	Y1-1	Y1-2	Y1-3	Y1-4	Y1-5	Sample	Y1-1	Y1-2	Y1-3	Y1-4	Y1-5
Major elements (wt%)						Trace elements (ppm)					
SiO <sub>2</sub>	71.71	72.18	71.64	72.84	71.28	Zr	75.02	75.86	80.47	86.33	74.46
TiO <sub>2</sub>	0.18	0.21	0.20	0.19	0.19	Nb	10.67	12.25	12.71	12.34	11.40
Al <sub>2</sub> O <sub>3</sub>	14.69	14.46	14.61	15.11	14.39	Mo	0.67	0.54	0.44	0.37	0.76
TFe <sub>2</sub> O <sub>3</sub>	2.11	1.67	1.85	1.68	2.00	Sn	13.13	11.32	11.64	12.18	12.01
MnO	0.10	0.06	0.07	0.08	0.10	Cs	10.57	11.78	14.01	17.54	19.30
MgO	0.28	0.47	0.50	0.35	0.42	Ba	199.67	195.63	232.72	224.80	231.54
CaO	1.07	0.94	0.92	1.09	1.09	La	18.61	21.28	23.72	22.22	21.96
Na <sub>2</sub> O	3.09	2.80	2.83	3.25	2.64	Ce	32.92	40.61	49.60	44.16	42.88
K <sub>2</sub> O	4.58	4.77	4.95	5.06	5.10	Pr	4.24	5.45	6.41	5.85	5.43
P <sub>2</sub> O <sub>5</sub>	0.18	0.18	0.18	0.18	0.17	Nd	16.66	21.42	25.10	22.51	20.96
LOI	1.09	1.19	1.09	0.71	1.47	Sm	3.65	4.31	5.20	4.76	4.40
Total	99.08	98.92	98.83	100.54	98.85	Eu	0.79	0.52	0.91	0.86	0.88
Na <sub>2</sub> O/K <sub>2</sub> O	0.67	0.59	0.57	0.64	0.52	Gd	3.27	3.49	4.33	4.12	3.79
Na <sub>2</sub> O+K <sub>2</sub> O	7.67	7.57	7.78	8.31	7.74	Tb	0.52	0.49	0.64	0.64	0.59
δ	2.05	1.96	2.11	2.31	2.12	Dy	2.77	2.20	3.00	3.24	2.91
A/NK	1.46	1.48	1.46	1.39	1.46	Ho	0.48	0.34	0.48	0.55	0.47
A/CNK	1.22	1.26	1.25	1.18	1.21	Er	1.39	0.90	1.32	1.57	1.27
Trace elements (ppm)						Tm	0.21	0.12	0.17	0.22	0.17
Li	83	120	152	104	92	Yb	1.40	0.75	1.10	1.51	1.09
Be	6.44	5.00	5.02	7.22	8.92	Lu	0.21	0.11	0.16	0.22	0.16
Sc	2.08	1.42	3.16	2.96	2.40	Hf	2.94	2.82	2.96	3.13	2.74
Ti	983	1160	1172	1168	1046	Ta	1.15	1.07	1.19	1.08	0.98
V	9.45	10.67	11.23	11.65	10.06	Bi	1.42	0.99	0.85	0.32	0.65
Cr	19.48	11.57	10.28	10.71	13.77	Th	7.93	12.32	12.86	11.74	10.80
Mn	1078	662	729	855	1276	U	14.53	3.74	4.44	4.39	5.26
Co	14.56	2.14	2.60	2.40	2.77	ΣREE	87.12	101.99	122.12	112.43	106.94
Ni	9.25	3.05	3.44	3.31	5.05	LREE	76.87	93.59	110.92	100.36	96.50
Cu	18.93	3.17	3.31	2.63	4.18	HREE	10.24	8.40	11.20	12.07	10.44
Zn	1038	41	42	52	58	LREE/HREE	7.51	11.15	9.91	8.31	9.24
Ga	17.61	16.56	17.92	17.79	16.52	Nb/Ta	9.25	11.44	10.64	11.42	11.67
Rb	250.5	212.5	298.9	278.9	305.1	La <sub>N</sub> /Yb <sub>N</sub>	9.53	20.26	15.40	10.56	14.49
Sr	63.34	43.39	68.57	68.33	74.54	δEu	0.69	0.40	0.57	0.58	0.64
Y	15.70	10.09	15.64	18.10	15.78	δCe	0.87	0.90	0.97	0.93	0.94

Note: A/CNK = molar ratio of Al<sub>2</sub>O<sub>3</sub>/(CaO+Na<sub>2</sub>O+K<sub>2</sub>O); A/NK = molar of Al<sub>2</sub>O<sub>3</sub>/(Na<sub>2</sub>O+K<sub>2</sub>O); δ = [w(K<sub>2</sub>O+Na<sub>2</sub>O)<sup>2</sup>]/[w(SiO<sub>2</sub>)-43]

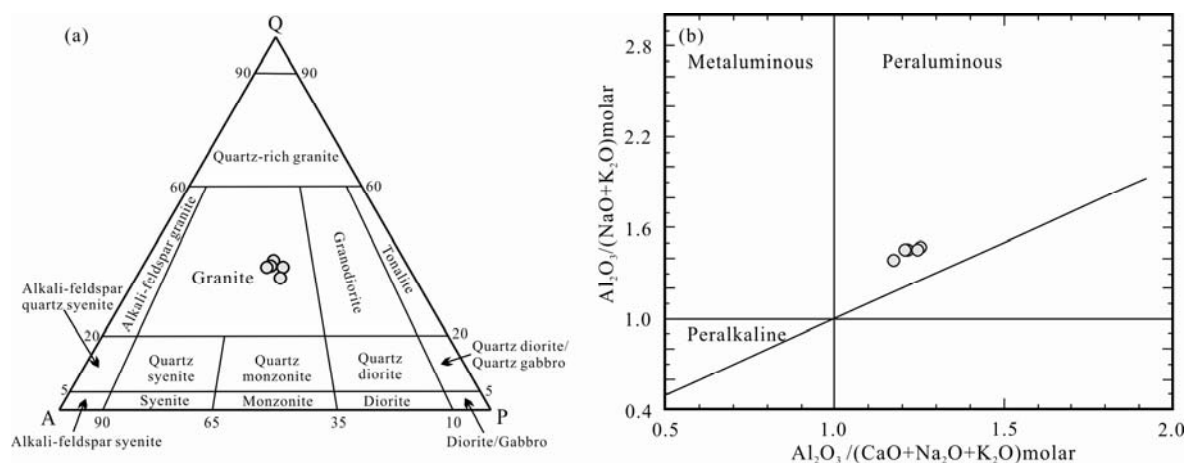


Fig. 7. Major elements classification of the Yangbishan gneissic granite.

(a), QAP classification diagram (after Streckisen, 1976), Q, A, P are quartz, alkali feldspar and plagioclase contents, respectively; (b), Al<sub>2</sub>O<sub>3</sub>/(Na<sub>2</sub>O + K<sub>2</sub>O) versus Al<sub>2</sub>O<sub>3</sub>/(CaO + Na<sub>2</sub>O + K<sub>2</sub>O) diagram (after Maniar and Piccoli, 1989).

(Fig. 8a), these samples are characterized by enrichment of LREEs, depletion of HREEs, and no obvious fractionation of the HREEs.

In the primitive mantle-normalized trace element spider diagram (Fig. 8b), these samples demonstrate the enrichment of some large ion lithophile elements (LILEs: Cs, Rb, and U), as well as a depletion of high field strength elements (HFSEs: Nb, Ta, Zr, Hf, and Ti).

### 5.3 Zircon Hf isotope compositions

Hf isotope analyses were conducted on the twenty zircon grains with determined U–Pb ages (Table 3 and Fig. 5). The two inherited zircons (1202–1488 Ma) have variable Hf isotopic compositions, with <sup>176</sup>Hf/<sup>177</sup>Hf ratios of 0.282264–0.281934, ε<sub>Hf</sub>(*t*) values of +7.9 and +1.4, *T*<sub>DM1</sub> values of 1.39–1.90 Ga, and *T*<sub>DM2</sub> values of 1.51–2.13 Ga. The ε<sub>Hf</sub>(*t*) values for 18 magmatic zircons are

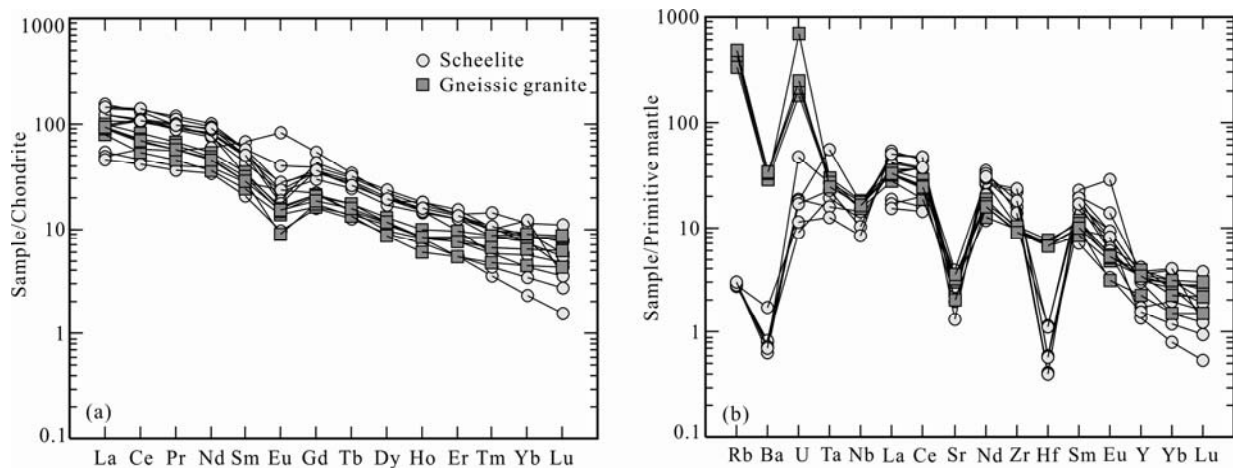


Fig. 8. Chondrite-normalized REE distribution patterns and primitive mantle-normalized spidergrams of gneissic granite and scheelite from the Yangbishan deposit. Chondrite-normalized and primitive mantle-normalized values are from Sun and McDonough (1989) and McDonough and Sun (1995), respectively.

**Table 3 Lu–Hf isotopic data for zircons from the gneissic granite (sample YBS4–1)**

Sample No.	Spot No. <sup>a</sup>	<sup>176</sup> Hf/ <sup>177</sup> Hf	1σ	<sup>176</sup> Lu/ <sup>177</sup> Hf	1σ	<sup>176</sup> Yb/ <sup>177</sup> Hf	1σ	Age(Ma)	Hf <sub>i</sub>	ε <sub>Hf</sub> (t)	T <sub>DM1</sub> (Ga)	T <sub>DM2</sub> (Ga)	f <sub>Lu/Hf</sub>
1	YBS4-1-2	0.282422	0.000017	0.000974	0.000047	0.038146	0.002027	521	0.282412	-1.3	1.17	1.56	-0.97
2	YBS4-1-3	0.282262	0.000016	0.001235	0.000010	0.043568	0.000538	523	0.282249	-7.0	1.41	1.92	-0.96
3	YBS4-1-5	0.282449	0.000016	0.000725	0.000011	0.026834	0.000345	523	0.282442	-0.2	1.13	1.49	-0.98
4	YBS4-1-6	0.282460	0.000017	0.001985	0.000022	0.069117	0.000971	530	0.282440	-0.1	1.15	1.49	-0.94
5	YBS4-1-7	0.282411	0.000015	0.000383	0.000010	0.014820	0.000448	522	0.282407	-1.4	1.17	1.57	-0.99
6	YBS4-1-8	0.282412	0.000017	0.000387	0.000009	0.016995	0.000357	522	0.282408	-1.4	1.17	1.57	-0.99
7	YBS4-1-12	0.282264	0.000021	0.000895	0.000002	0.033214	0.000087	1202	0.282243	7.9	1.39	1.51	-0.97
8	YBS4-1-13	0.282327	0.000017	0.000659	0.000016	0.025302	0.000668	522	0.282321	-4.5	1.29	1.77	-0.98
9	YBS4-1-17	0.282319	0.000014	0.000081	0.000003	0.003366	0.000114	523	0.282319	-4.5	1.29	1.77	-1.00
10	YBS4-1-22	0.282039	0.000021	0.001345	0.000007	0.045618	0.000340	522	0.282026	-14.9	1.72	2.42	-0.96
11	YBS4-1-23	0.282409	0.000015	0.000568	0.000027	0.020105	0.000793	525	0.282403	-1.5	1.18	1.58	-0.98
12	YBS4-1-29	0.282443	0.000015	0.000902	0.000063	0.033857	0.002434	516	0.282435	-0.6	1.14	1.52	-0.97
13	YBS4-1-30	0.282282	0.000018	0.001115	0.000023	0.043714	0.000823	524	0.282271	-6.2	1.37	1.88	-0.97
14	YBS4-1-31	0.281934	0.000019	0.001984	0.000099	0.073449	0.004072	1488	0.281878	1.4	1.90	2.13	-0.94
15	YBS4-1-32	0.282467	0.000017	0.001325	0.000065	0.051701	0.003666	525	0.282454	0.3	1.12	1.47	-0.96
16	YBS4-1-33	0.282344	0.000016	0.001113	0.000044	0.040317	0.002007	518	0.282333	-4.1	1.29	1.74	-0.97
17	YBS4-1-34	0.282502	0.000015	0.001791	0.000047	0.072282	0.001632	516	0.282485	1.2	1.08	1.40	-0.95
18	YBS4-1-35	0.282564	0.000025	0.004931	0.000154	0.208325	0.006247	524	0.282515	2.5	1.09	1.33	-0.85
19	YBS4-1-37	0.282445	0.000020	0.001886	0.000108	0.071745	0.003866	540	0.282426	-0.4	1.17	1.52	-0.94
20	YBS4-1-38	0.282310	0.000016	0.000359	0.000018	0.015196	0.000774	529	0.282306	-4.8	1.31	1.79	-0.99

Note: <sup>a</sup> Numbers indicate the same spot localities as those with the spot numbers in Table 1 and Figure 5.

between -14.9 and +2.5, and the corresponding <sup>176</sup>Hf/<sup>177</sup>Hf, T<sub>DM1</sub> and T<sub>DM2</sub> values vary from 0.282262 to 0.282564, 1.08 to 1.72 Ga, and 1.33 to 2.42 Ga, respectively.

#### 5.4 Rare earth and trace element compositions of the scheelite

Rare earth and trace element contents of the scheelite in the Yangbishan are listed in Table 4. The total rare earth element contents (ΣREE) of the samples range from 66.4 ppm to 202.06 ppm, while LREEs are relatively enriched as compared with HREEs (ΣLREE = 58.38–183.59 ppm; ΣHREE = 8.02–20.86 ppm; LREE/HREE = 4.52–16.01). Fractionation of LREEs and HREEs is clear [(La/Yb)<sub>N</sub> = 10.76–26.63]. Europium displays a mainly negative anomaly (δEu = 0.38–0.69, mean 0.57), and cerium anomaly is not obvious (δCe = 0.99–1.12, mean 1.06). In the chondrite-normalized REE diagram (Fig. 8a), samples

are characterized by enrichment of LREEs and depletion of HREEs.

In the Table 4, mean contents of some trace elements in the scheelite, such as Zn, Sr, and Pb, are more than 10 ppm, while those of some other elements are more than 1 ppm, for examples V, Cr, Ni, Ga, Rb, Zr, Nb, Ba, Hf, Ta, and Pb. It's worth pointing out that Ca<sup>2+</sup> can be isomorphously replaced by Sr, Pb, and Ba, and W<sup>6+</sup> can be isomorphously replaced by Cr, V, Ga, and Ni. In the chondrite-normalized REE diagram (Fig. 8a) and the primitive mantle-normalized trace element spider diagram (Fig. 8b), the scheelite samples and gneissic granite of the Yangbishan deposit show similar distribution patterns.

## 6 Discussion

### 6.1 Genesis and age of tungsten mineralization

The tungsten mineralization in the Yangbishan deposit

**Table 4 Trace element compositions of the scheelite in the Yangbishan deposit**

Sample	YB-11-1	YB-11-2	YB-8	Y1-6	Y1-4	YB-2	YBS01	YBS1-3	YBS42-1	YBS42-2	YBS42-3	Mean
V	2.47	2.21	1.49	2.86	2.84	2.22	—	—	—	—	—	2.35
Cr	4.31	4.15	2.57	2.69	4.09	2.09	—	—	—	—	—	3.32
Ni	7.82	4.72	6.36	2.14	4.46	2.32	—	—	—	—	—	4.64
Zn	26.70	6.77	9.69	7.75	8.80	10.76	—	—	—	—	—	11.74
Ga	1.57	1.31	2.30	1.54	1.36	0.94	—	—	—	—	—	1.50
Rb	1.76	1.92	1.89	1.87	1.71	1.76	—	—	—	—	—	1.82
Sr	50.55	46.87	28.23	41.38	82.31	57.59	—	—	—	—	—	51.15
Zr	13.08	6.75	12.56	4.49	4.61	6.48	—	—	—	—	—	7.99
Nb	12.49	7.25	10.67	10.21	8.59	5.88	—	—	—	—	—	9.18
Cs	0.22	0.18	0.38	0.58	2.29	0.48	—	—	—	—	—	0.69
Ba	5.76	5.03	4.93	4.45	5.55	11.97	—	—	—	—	—	6.28
Hf	3.19	6.81	5.50	4.24	4.91	7.09	—	—	—	—	—	5.29
Ta	2.21	0.92	1.07	0.64	0.77	0.51	—	—	—	—	—	1.02
U	0.38	0.35	0.97	0.39	0.19	0.24	—	—	—	—	—	0.42
Pb	7.80	6.77	8.57	12.28	11.13	14.98	—	—	—	—	—	10.25
La	29.02	28.19	33.83	33.19	24.90	36.04	12.50	11.50	22.80	22.20	10.50	15.90
Ce	66.22	64.28	83.55	82.64	62.32	77.84	27.80	35.10	66.40	64.70	25.30	43.86
Pr	8.58	8.30	10.26	11.17	8.52	9.10	3.72	5.25	9.29	9.11	3.39	6.15
Nd	36.19	34.63	43.59	46.39	38.40	35.32	17.70	27.20	40.20	41.60	15.50	28.44
Sm	7.23	6.53	8.63	8.66	7.67	4.99	4.22	10.10	8.58	7.49	3.14	6.71
Eu	1.57	1.31	2.30	1.54	1.36	0.94	1.36	4.78	1.08	1.00	0.55	1.75
Gd	6.93	5.93	7.70	7.33	7.06	4.35	4.41	10.80	8.65	7.39	3.24	6.90
Tb	1.04	0.90	1.14	1.05	0.97	0.54	0.55	1.25	1.16	0.97	0.46	0.88
Dy	4.75	4.28	5.53	4.99	4.91	2.43	2.83	5.35	5.90	4.77	2.25	4.22
Ho	1.01	0.81	0.93	0.89	0.84	0.46	0.46	0.82	1.02	0.89	0.41	0.72
Er	2.29	2.03	2.25	2.21	2.03	1.24	0.90	1.60	2.47	2.20	0.90	1.61
Tm	0.36	0.25	0.25	0.24	0.21	0.15	0.09	0.15	0.26	0.27	0.11	0.18
Yb	1.93	1.44	2.02	1.55	1.29	0.97	0.39	0.74	1.26	1.48	0.58	0.89
Lu	0.28	0.20	0.09	0.15	0.11	0.12	0.04	0.09	0.14	0.19	0.07	0.11
Y	16.24	14.43	17.18	16.14	14.37	7.75	6.29	13.50	19.20	14.60	7.15	12.15
ΣREE	167.41	159.09	202.06	202.00	160.60	174.48	76.97	114.73	169.21	164.26	66.40	118.31
LREE	148.81	143.24	182.15	183.59	143.17	164.22	67.30	93.93	148.35	146.10	58.38	102.81
HREE	18.59	15.84	19.91	18.41	17.43	10.26	9.67	20.80	20.86	18.16	8.02	15.50
LREE/HREE	8.00	9.04	9.15	9.97	8.21	16.01	6.96	4.52	7.11	8.05	7.28	6.78
La <sub>N</sub> /Yb <sub>N</sub>	10.79	14.01	12.01	15.33	13.82	26.63	22.99	11.15	12.98	10.76	12.99	14.17
δEu	0.67	0.63	0.84	0.58	0.56	0.60	0.96	1.39	0.38	0.41	0.52	0.73
δCe	1.02	1.02	1.09	1.05	1.05	1.03	0.99	1.11	1.12	1.12	1.03	1.07
Rb/Sr	0.03	0.04	0.07	0.05	0.02	0.03	—	—	—	—	—	0.04
Nb/Ta	5.65	7.91	9.93	15.91	11.1	11.54	—	—	—	—	—	10.34
Zr/Hf	4.1	0.99	2.28	1.06	0.94	0.91	—	—	—	—	—	1.71

is an example of contact metasomatic, or skarn-type, mineralization. The primary lines of evidence are that (i) tungsten ore bodies occur in the contact zone between the gneissic granite and the marble of the Dapandao Formation; (ii) tungsten ore bodies are controlled by that contact zone and present as veins, lenses, or layer-like shapes; (iii) the tungsten ore has similar mineral assemblages, paragenesis, ore textures, and ore structures to the typical skarn deposit; and (iv) the skarn is closely associated with the tungsten mineralization, and the wall-rock alteration occurs on both sides of the contact zone. This view is also supported by comparisons between the Yangbishan tungsten deposit and typical skarn-type tungsten deposits in China (Table 5).

The LA-ICP-MS U–Pb dating of zircons from the gneissic granite that is genetically associated with the Yangbishan tungsten mineralization indicates an emplacement age of  $520.6 \pm 2.8$  Ma. Because the Yangbishan skarn ores are genetically related to the emplacement of the granite, it can be inferred that the mineralization also took place c. 520 Ma (early Paleozoic). The Yangbishan deposit may be the earliest tungsten

deposit discovered in northeast China (Table 6), which implies the potential for further Paleozoic tungsten discoveries in the eastern portion of the CAOB.

## 6.2 Nature of the ore-forming fluid

Because the scheelite is rich in certain trace elements (e.g., Nb and Ta) and REEs, and can inherit its REE signature from the ore-forming fluid present during its genesis (Ghaderi et al., 1999), these elements can be used to trace the sources and geochemistry of the relevant ore-forming hydrothermal system (Eichhorn et al., 1997; Ghaderi et al., 1999; Brugger et al., 2000, 2002; Xiong Dexin et al., 2006; Ren Yunsheng et al., 2010a).

Analytical results presented in this paper show that the LREE/HREE ratios of the scheelite in Yangbishan range from 4.52 to 16.01, with a mean of 8.66, which shows that the scheelite samples have typical right-dipping REE patterns: they are enriched in LREEs and heavily depleted in HREEs, with a negative Eu anomaly. The geochemical characteristics of the scheelite samples from the Yangbishan deposit are similar to those from the Baishilazi, Zhuxi, Jitoushan, and Baizhangyan deposits,

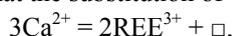
**Table 5 Geological characteristic comparison between the Yangbishan and some typical skarn tungsten deposits in China**

Name	Yangbishan Fe-W deposit	Shizhuyuan W-Sn polymetallic deposit	Xianglushan W deposit	Baishilazi W deposit	Cuihongshan W-Mo polymetallic deposit
Location	Heilongjiang Province	Hunan Province	Jiangxi Province	Jilin Province	Heilongjiang Province
Ore-controlling structure	Controlled by contact zone between gneissic granite and marble	Controlled by contact zone between alkali-feldspar granite and limestone	Controlled by contact zone between biotite granite and limestone	Controlled by contact zone between quartz diorite and marble	Controlled by contact zone between monzonitic granite and marble
Host rock	Diopside skarn	Garnet diopside skarn	Diopside skarn	Garnet skarn	Diopside garnet skarn
Ore body shape	Vein, lenticular and quasi-bedded forms	lenticular and quasi-bedded forms	lenticular forms	Vein and lenticular forms	Vein, saccate and lenticular forms
Ore textures and structures	Euhedral-subhedral granular texture, metasomatic relict texture, disseminated and vein structures	Euhedral-subhedral granular texture, metasomatic relict texture, disseminated, banded and vein structures	Euhedral-subhedral granular texture, metasomatic relict texture, exsolution texture, disseminated and veinlet structures	Euhedral-subhedral granular texture, metasomatic relict, dissolution, and skeletal textures, disseminated and veinlet structures	Euhedral-subhedral granular texture, metasomatic relict texture, disseminated, veinlet and breccia structures
Metallic minerals	Scheelite, magnetite, pyrrhotite, pyrite, chalcocopyrite, sphalerite and cassiterite	Magnetite, scheelite, wolframite, molybdenite, pyrrhotite, sphalerite and chalcocopyrite	Scheelite, chalcocopyrite, pyrrhotite, pyrite, sphalerite and galena.	Scheelite, chalcocopyrite, pyrrhotite and pyrite	Magnetite, molybdenite, scheelite, sphalerite, galena, chalcocopyrite, cassiterite, arsenopyrite, pyrite and pyrrhotite
Nonmetallic minerals	Augite, diopside, quartz, grossularite, plagioclase, scapolite and fluorite	Garnet, clinopyroxene, idocrase, epidote, tourmaline, actinolite, potassium feldspar, plagioclase, fluorite, quartz and muscovite	Garnet, diopside, tremolite, quartz and calcite	Grossularite, andradite, diopside, epidote, calcite and quartz	Diopside, garnet, phlogopite, humite, ilvaite, idocrase, actinolite, epidote, tremolite, fluorite, quartz, chlorite and calcite
Wall rock alteration	Skarnization, silicification, chloritization, carbonatation, epidotization, fluoritization	Skarnization, greisenization, silicification, fluoritization, epidotization, chloritization	Skarnization, greisenization, silicification, potassic alteration, chloritization, fluoritization, carbonatation, actinolitization and sericitization	Skarnization, silicification, chloritization, sericitization, carbonatation	Skarnization, silicification, sericitization and carbonatation
Formation age	Cambrian	Jurassic	Cretaceous	Jurassic	Jurassic
References	This study	Zhu Xinyou et al., 2015	Wu Shenghua et al., 2014	Zhao Hualei et al., 2011	Hao Yujie et al., 2013

**Table 6 Metallogenic epoch of representative tungsten deposits in NE China**

Name	Mine types	Deposit type	Size	Metallogenic epoch (Ma)	Rock tested	Test method	References
Yangbishan	Fe-W	sedimento-metamorphic and skarn	medium	520.6 ± 2.8	gneissic granite	zircon U-Pb	This study
Yangjingou	W	lode	large	249.4 ± 2.7 230.8 ± 1.2	granodiorite muscovite	zircon U-Pb Ar-Ar	Zhao Hualei, 2014
Cuihongshan	W-Mo polymetal	skarn	large	198.9 ± 3.7	molybdenite	Re-Os	Hao Yujie et al., 2013
Wudaogou	W	lode	medium	251.7 ± 2.9	scheelite	Sm-Nd	Unpublished data
Baishilazi	W	lode	medium	198.3 ± 0.8	quartz diorite	zircon U-Pb	Zhao Hualei et al., 2011
Sanjiazi	W	skarn	medium	172.4 ± 1.8	biotite adamellite	zircon U-Pb	Ren Yunsheng et al., 2010b
Gongpengzi	Cu-Zn-W	skarn	medium	172.2 ± 1.6	granodiorite	zircon U-Pb	Wang Zhigang, 2012
Honghuaerji	W polymetal	lode	large	179.2 ± 1.8 176.8 ± 2.2	biotite granite molybdenite	zircon U-Pb Re-Os	Xiang Anping et al., 2014
Shamai	W	lode	medium	137.9 ± 1.7 139.1 ± 0.9	wolframite biotite granite	Sm-Nd zircon U-Pb	Li Junjian et al., 2016

which also have right-dipping REE patterns (Song et al., 2014; Zhao Hualei, 2014; Hu Zhenghua, 2015). Zeng Zhigang et al. (1998) and Song et al. (2014) determined that the substitution of



where  $\square$  is a Ca-site vacancy (Ghaderi et al., 1999; Brugger et al., 2000), could explain the REE right-dipping patterns, and that the patterns were inherited mainly from the ore-forming fluid.

Figure 4 shows that the Yangbishan scheelite was precipitated during the oxide stage that followed the skarn stage. Several studies have shown that garnets and pyroxenes in metamorphic and magmatic systems are typically enriched in HREEs and depleted in LREEs (Graunch, 1989; Bea et al., 1997; Zhang Hongfu et al., 2000; Boyd et al., 2004). At Yangbishan, this probably means that the formation of the skarn minerals, such as garnet and pyroxene, would have resulted in residual

fluids that were rich in LREEs and poor in HREEs. Scheelites inherit their REE patterns primarily from the ore-forming fluid (Sylvester and Ghaderi, 1997; Ghaderi et al., 1999; Brugger et al., 2000; Dostal et al., 2009; Peng Jiantang et al., 2010), so it is reasonable that their typical right-dipping REE patterns would be controlled by the earlier precipitation of skarn minerals, which left the residual fluids depleted in HREEs (Graunch, 1989; Bea et al., 1997; Zhang Hongfu et al., 2000; Boyd et al., 2004). The REE features of the gneissic granite at Yangbishan are consistent with those of the scheelite (Fig. 8a), which indicates that the ore fluids originated from the granite magma. The gneissic granite can be considered the metallogenetic rock for the Yangbishan deposit.

The scheelite samples from different types of deposits can be plotted on a triangular LREE–MREE–HREE diagram (Fig. 9). In this figure, most of the Yangbishan scheelite samples are located within the skarn-type domain, indicating that it is a skarn deposit and therefore similar to the Baishilazi skarn deposit in the Yanbian area.

The typical right-dipping REE pattern of the Yangbishan skarn deposit, and its lack of enrichment in MREEs, indicates that the minerals of the deposit precipitated out of a fluid with high  $\text{Eu}^{2+}/\text{Eu}^{3+}$  ratios (Hazarika et al., 2016). Song et al. (2014) suggested that a high concentration of  $\text{Eu}^{2+}$  relative to  $\text{Eu}^{3+}$  in a

hydrothermal solution would result in a positive Eu anomaly in the resulting REE pattern (e.g., the Yangjingou tungsten deposit; Ren Yunsheng et al., 2010a). By contrast, a high concentration of  $\text{Eu}^{3+}$  relative to  $\text{Eu}^{2+}$  would result in a negative Eu anomaly. Ghaderi et al. (1999) suggested that Eu anomalies observed in the scheelite were inherited from their genetic fluids. As mentioned above, the scheelite in the Yangbishan deposit inherited its REE pattern primarily from its ore-forming fluid, which in turn inherited its REE pattern from the metallogenetic gneissic granite. Although the Yangbishan scheelite samples do not generally show positive Eu anomalies (0.38–1.39, mean 0.68), the negative anomaly is weaker than those in the gneissic granites (0.40–0.69, mean 0.58) (Fig. 8a). We therefore conclude that the scheelite in the Yangbishan deposit precipitated under reducing conditions from hydrothermal solutions with a high concentration of  $\text{Eu}^{2+}$ . There are no obvious  $\delta\text{Ce}$  anomalies in the Yangbishan scheelite ( $\delta\text{Ce} = 0.99\text{--}1.12$ , mean 1.05), which is consistent with a reducing environment for the ore-forming fluids. In addition, the Yangbishan scheelite has close paragenetic relationships with pyrrhotite, pyrite, and chalcopyrite (Fig. 3d–e), which also indicates a reducing environment during the main stage of mineralization. In fact, we have previously detected  $\text{CH}_4$  by laser Raman spectroscopy in some fluid inclusions in the Yangbishan deposit (unpublished data). Taken together, these lines of evidence indicate that the ore-forming fluid of this deposit was a reducing system.

The concentrations of most trace elements (e.g., Rb, Nb, Ta, Zr, and Hf) in the Yangbishan scheelite samples are clearly higher than in the scheelite samples of the Yangjingou tungsten deposit in the Yanbian area, while the concentrations of Sr are lower than in the scheelite of the Yangjingou tungsten deposit or the Baizhangyan and Jitoushan tungsten–molybdenum deposits (Table 7). As a whole, the trace element contents of the Yangbishan scheelite are similar to those of the scheelite in the Zhuxi polymetallic deposit. In addition, Yangbishan scheelite samples have higher Rb/Sr and Nb/Ta ratios (means of 0.04 and 10.34, respectively) and lower Zr/Hf ratios (mean of 1.71) than those in the other deposits (Table 7). Previous researchers have suggested that the ore-forming materials in the Zhuxi deposit are not exclusively magmatic in origin, but might have resulted from interactions between magmatic hydrothermal solutions and surrounding rocks (Hu Zhenghua, 2015). Based on comparisons between the trace element contents of the Yangbishan scheelite and those of primitive mantle (Rb/Sr = 0.031, Nb/Ta = 14, Zr/Hf = 30.74; Taylor and McLennan, 1985), it can be concluded that the ore-forming materials of the Yangbishan tungsten

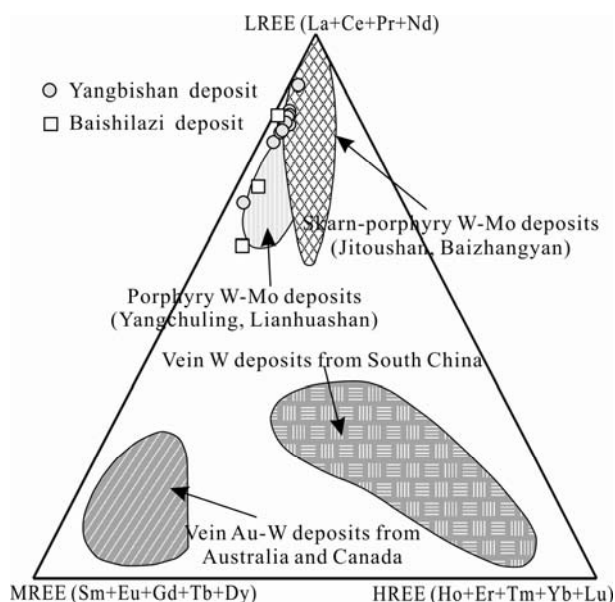


Fig. 9. Triangular LREE–MREE–HREE diagram of the scheelite from the Yangbishan deposit (after Song et al., 2014).

The data of scheelite from skarn–porphyry W–Mo, Skarn W, vein-type Au–W, vein-type W, and porphyry-type W–Mo deposits were taken from Henderson (1985), Zhang Yuxue et al. (1990), Raimbault et al. (1993), Sylvester and Ghaderi (1997), Ghaderi et al. (1999), Brugger et al. (2000), Dostal et al. (2009), Peng Jiantang et al. (2010), Song et al. (2014), and Zhao (2014), respectively.

**Table 7 Trace element compositions of the Yangbishan scheelite**

Name	Yangbishan		Yangjingou		Baizhangyan		Jitoushan		Zhuxi	
	mean	No.	mean	No.	mean	No.	mean	No.	mean	No.
V	2.35	6	3.17	6	—	—	—	—	0.02	11
Cr	3.32	6	14.85	6	—	—	—	—	17.26	15
Ni	4.64	6	8.96	6	—	—	—	—	1.05	8
Zn	11.74	6	—	—	10.22	18	8.86	17	1.52	12
Ga	1.50	6	1.06	6	—	—	—	—	0.34	14
Rb	1.82	6	0.17	6	0.11	22	0.19	16	0.06	10
Sr	51.15	6	193	6	115.97	35	303.69	35	43.12	15
Zr	7.99	6	0.69	6	—	—	—	—	3.45	15
Nb	9.18	6	0.14	6	—	—	—	—	24.96	15
Cs	0.69	6	—	—	—	—	—	—	0.11	11
Ba	6.28	6	3.98	6	0.72	35	0.34	34	0.11	11
Hf	5.29	6	0.09	6	—	—	—	—	0.7	15
Ta	1.02	6	0.03	6	—	—	—	—	4.87	15
U	0.42	6	0.15	6	—	—	—	—	1.23	15
Pb	10.25	6	1.08	6	8.64	35	2.26	35	1.85	15
*(Rb/Sr)	39.84	6	0.1	6	1.06	22	0.68	16	1.36	10
Nb/Ta	10.34	6	4	6	—	—	—	—	4.85	15
Zr/Hf	1.71	6	6.96	6	—	—	—	—	5.04	15
References	This study		Ren Yunsheng et al., 2010a		Song et al., 2014		Song et al., 2014		Hu Zhenghua, 2015	

mineralization are also related to interactions between magmatic hydrothermal solutions and their surrounding rocks, similar to the Shangfang skarn tungsten deposit and the Zhuxi skarn tungsten polymetallic deposit (Chen Runsheng, 2013; Hu Zhenghua, 2015). This conclusion has been confirmed by new  $\delta^{18}\text{O}$  values and  $\delta\text{D}$  values from 11 quartz samples from the Yangbishan deposit located during the major tungsten mineralization stage (unpublished data). The measured  $\delta^{18}\text{O}$  values for the tungsten-bearing quartz range from 11‰ to 15‰, and the estimated  $\delta^{18}\text{O}$  values for fluids range from 5 to 9‰. The  $\delta\text{D}$  values for fluid inclusions of the tungsten-bearing quartz range from  $-121\text{‰}$  to  $-66\text{‰}$ . These results suggest that the ore-forming fluid was derived mainly from the magmatic system and subordinately from the nearby carbonate strata, with minor organic matter contamination.

In summary, the Yangbishan scheelite samples have similar geochemical features to those in the Zhuxi, Baizhangyan, and Jitoushan deposits: enrichment of LREEs, depletion of HREEs, and right-dipping chondrite-normalized REE patterns. The Yangbishan scheelites inherited their REE features from ore-forming fluids, which implies that  $\text{REE}^{3+}$  replaced  $\text{Ca}^{2+}$  and entered the scheelite. Compared with the metallogenic granite, the Yangbishan scheelite samples have weak negative Eu anomalies and no obvious Ce anomalies, which indicate that the scheelite formed in a reducing environment. The fact that the trace element characteristics of the Yangbishan scheelite differ from those of the Yangjingou deposit implies that the Yangbishan ore-forming materials resulted from interactions between magmatic hydrothermal solutions and the surrounding rocks, and this is consistent with the LREE–MREE–HREE data (Fig. 9).

### 6.3 Petrogenesis and source of the gneissic granite

The geochemical characteristics of the Yangbishan gneissic granite indicate that it is a peraluminous high-Si, sub-alkaline granite with an ACNK ratio  $> 1.1$  and relatively high values for its  $\text{K}_2\text{O}/\text{Na}_2\text{O}$ , Rb/Sr, and Rb/Ba ratios (Table 2 and Fig. 7b). In primitive mantle-normalized trace element patterns (Fig. 8b), the granite samples showed enrichments in Rb, U, and Th, and negative anomalies in Ba, Sr, Nb, and Ti. The granite has a relatively low total REE content, clearly fractionated LREEs and HREEs, and strong Eu negative anomalies. In the  $\text{Al}_2\text{O}_3\text{--SiO}_2$  and  $\text{P}_2\text{O}_5\text{--SiO}_2$  diagrams (Fig. 10a and b), the Yangbishan gneissic granite is not consistent with the trends of I-type granites. Petrographic observation show that the gneissic granite contains muscovite, biotite, and minor garnet, instead of amphibole, which confirms that it is not an I-type granite. In the  $\text{Na}_2\text{O--K}_2\text{O}$  and  $\text{Na}_2\text{O--K}_2\text{O--}(10000 \times \text{Ga}/\text{Al})$  diagrams (Fig. 10c and d), the granite samples plot in or near the field of A-type or S-type granites. The zirconium saturation thermometer (Watson and Harrison, 1983) yielded a temperature of  $738\text{--}750^\circ\text{C}$  for the Yangbishan granite. Given that inherited zircons in the samples indicate that the magma was saturated with zirconium (Table 1), the zirconium saturation temperature may represent the upper limit of the initial temperature of the granite magma (Miller et al., 2003). The zirconium saturation temperature of the Yangbishan granite is lower than that of typical A-type granite (Zhang Zhenjie et al., 2016; Zhu Decheng et al., 2016), and closer to the average zirconium saturation temperature of S-type granite, which is  $764^\circ\text{C}$  (King et al., 1997). The granite's HFSE contents are relatively low, and the total content of Ce + Zr + Y + Nb is 134.32–160.94 ppm, far below the 350-ppm lowest limit for an A-type granite (Whalen et al., 1987). The above data and observations indicate that the Yangbishan

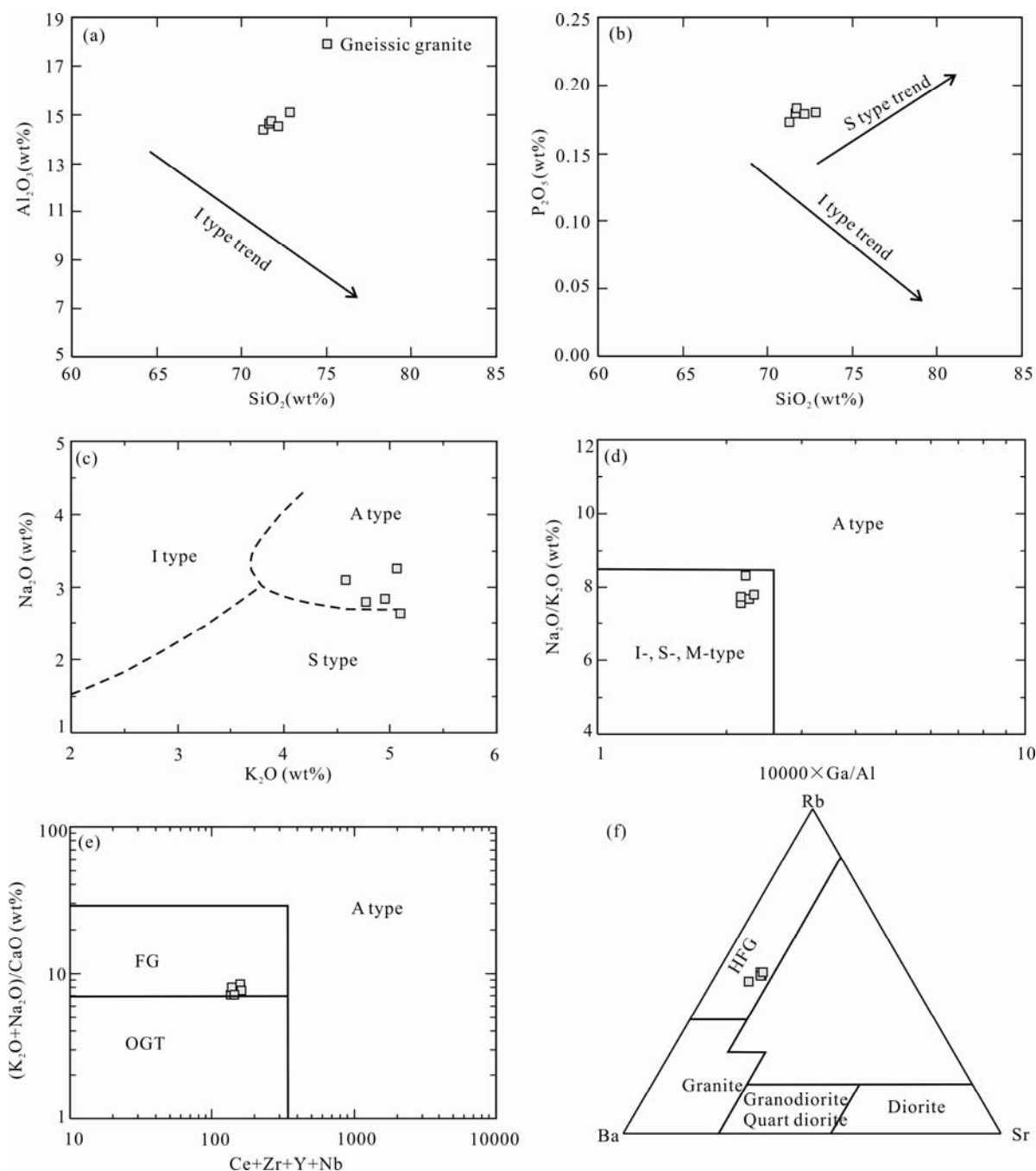


Fig. 10. (a),  $\text{Al}_2\text{O}_3$  vs  $\text{SiO}_2$  diagram; (b),  $\text{P}_2\text{O}_5$  vs  $\text{SiO}_2$  diagram; (c),  $\text{Na}_2\text{O}$  vs  $\text{K}_2\text{O}$  diagram; (d),  $\text{Na}_2\text{O}/\text{K}_2\text{O}$  vs  $10000 \times \text{Ga}/\text{Al}$  diagram; (e),  $(\text{K}_2\text{O} + \text{Na}_2\text{O})/\text{CaO}$  vs  $\text{Ce} + \text{Zr} + \text{Y} + \text{Nb}$  diagram and (f), Rb–Ba–Sr diagram.

a and b after Chappell and White (1992); c after Boynton (1984); d and e after Whalen et al. (1987); f after Müller and Groves (1998). FG, fractionated felsic granites; OGT, unfractionated I-, S- and M-type granites.

gneissic granite is not the A-type granite. The CIPW Norm of the granite includes quartz, anorthite, sodium feldspar, orthoclase, and corundum (2.74–3.49 mol%), which suggests that the granite is an aluminum- and silicon-oversaturated S-type granite. In the  $(\text{Na}_2\text{O} + \text{K}_2\text{O})/\text{CaO}$ – $(\text{Ce} + \text{Zr} + \text{Y} + \text{Nb})$  and Rb–Ba–Sr diagrams (Fig. 10e and f), the samples plot in the highly fractionated granite area. In summary, the Yangbishan gneissic granite should be classified as a highly fractionated S-type

granite.

The Yangbishan granitic rocks that were analyzed for this study are rich in Si but poor in Ca, Fe, Mg, and the transition elements (e.g. Sc, Ti, and Cr). These results indicate that the granitic magmas formed by partial melting of the crust, which is consistent with the presence of older, inherited zircons in the granite. Moreover, the Rb/Sr ratios of five samples of Yangbishan granite range from 3.95 to 4.90 (mean 4.28) and the Rb/Nd ratios are

9.91–15.03 (mean 12.76), all of which are higher than those found in the upper crust of eastern China (0.32 and 6.8, respectively; Gao Shan et al., 1999) and in the upper crust globally (0.32 and 4.5, respectively; Taylor and McLennan, 1985). These data support the conclusion that the Yangbishan granite was derived from a relatively mature crust.

The Hf isotopes of the zircons from the Yangbishan granitic rocks provide further constraints on the nature of the magma source. For example, all magmatic zircons from the Yangbishan granite samples have  $\varepsilon_{\text{Hf}}(t)$  values of  $-14.9$  to  $+2.5$  and plot between the depleted mantle and the chondrite line in the  $\varepsilon_{\text{Hf}}(t)$  vs.  $t$  diagram (Fig. 11). This, in combination with the  $T_{\text{DM2}}$  age of 1.33–2.42 Ga, suggests that the primary magma from which the Yangbishan granite was derived could have originated primarily from the partial melting of an “old” source. Such “old” crustal growth might have taken place during the Paleo–Mesoproterozoic eras. However, the Yangbishan granite samples show a wide range of magmatic zircon Hf

isotopic compositions, with  $\varepsilon_{\text{Hf}}(t) = -14.9$  to  $+2.5$  and  $T_{\text{DM2}} = 1.33$ – $2.42$  Ga. This precludes a simple, common evolution by closed-system fractionation processes, since such mechanisms cannot produce such variable isotopic compositions (Yang et al., 2008). Instead, wall-rock assimilation or magma mixing can reasonably account for isotopic variations during magmatic evolution (Yang et al., 2008, 2015; Sun Zhenjun et al., 2015). Mixing between mafic and felsic magma does not appear to have been a dominant mechanism, since the expected evidence is lacking, such as mafic microgranular enclaves. Furthermore, the Yangbishan granite contains inherited zircons with ages of 1812–1176 Ma, indicating that some crustal assimilation did take place and therefore supporting previous research (Bi et al., 2014). Taken together, it's believable that the petrogenesis of the Yangbishan granite was the result of the combined processes of crustal assimilation and fractional crystallization, and that primary magmas of these granitoids originated from the partial melting of a Paleo–Mesoproterozoic accreted lower crust source.

In the  $\text{CaO}/\text{Na}_2\text{O}-\text{Al}_2\text{O}_3/\text{TiO}_2$  diagram (Fig. 12a), the Yangbishan granite samples plot near argillaceous rock, implying that the source may have originally been argillaceous. In the  $\text{Rb}/\text{Ba}-\text{Rb}/\text{Sr}$  diagram (Fig. 12b), all the samples plot in the clay-enriched field and they have compositions similar to those of mudstone melts, indicating that the granite was derived mainly from the partial melting of what was originally a clay-rich mudstone. In general, there are fewer detrital zircon grains in clay-rich sedimentary rocks than in sedimentary rocks such as coarse sandstones, and Rb contents are relatively high in argillaceous rocks because of the mica. Therefore, the Zr contents would be relatively low in an S-type granite that formed from the partial melting of metamorphosed clay-rich sedimentary rocks (Patchett et al., 1984), while the Rb contents would be relatively high

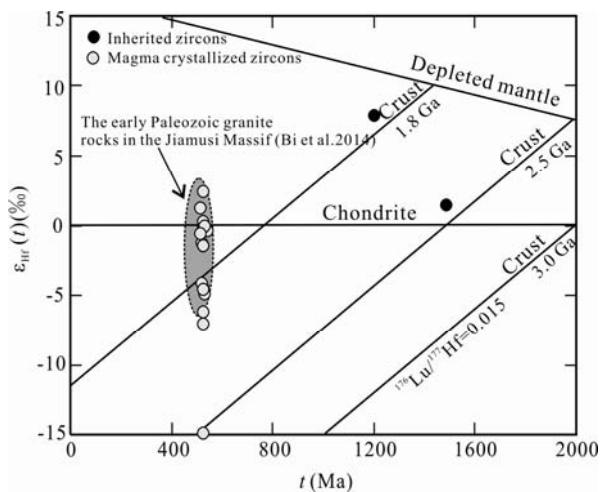


Fig. 11.  $\varepsilon_{\text{Hf}}(t)$  vs.  $t$  diagram of the Yangbishan gneissic granite.

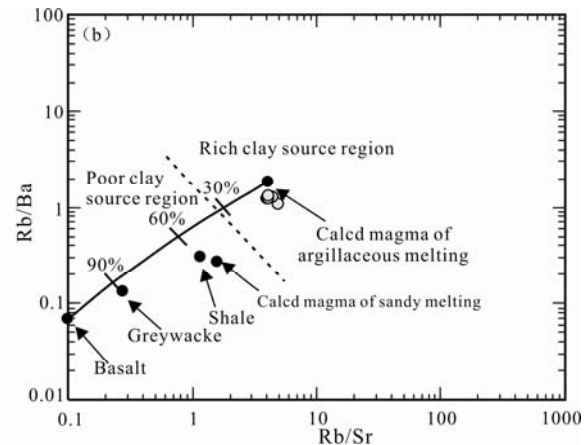
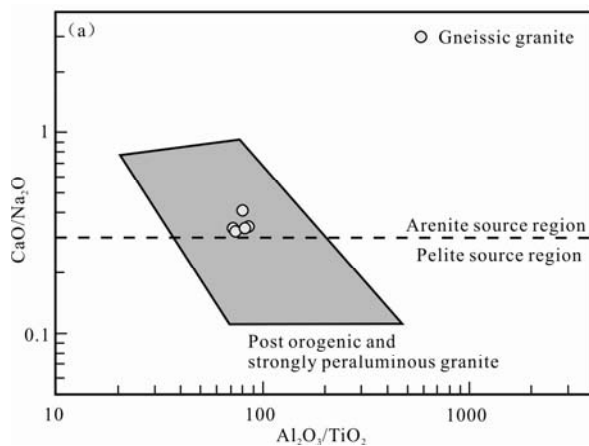


Fig. 12.  $\text{CaO}/\text{Na}_2\text{O}-\text{Al}_2\text{O}_3/\text{TiO}_2$  diagram (a) and  $\text{Rb}/\text{Ba}-\text{Rb}/\text{Sr}$  diagram (b) of gneissic granite from the Yangbishan deposit (after Sylvester, 1998).

(Liu Yingjun et al., 1982). The Yangbishan granite has relatively low Zr (75–86 ppm) but high Rb contents (213–305 ppm), consistent with the proposition that it originated from a metamorphosed clay-rich sedimentary source, rather than from a high degree of fractionation of a mafic magma.

The regional geology near the study location indicates that the Yangbishan granite intruded into the khondalite series of the Dapandao Formation of the Xingdong Group. The wall-rock was a complex of Al-rich graphite-bearing paragneisses that were originally muddy or silty sands that formed in a reducing environment (HBGMR, 1993; Dong Ce and Zhou Jianbo, 2012). Previous research has dated the Dapandao Formation to the Mesoproterozoic (HBGMR, 1993), and the latest data reveal that the deposition time of the Dapandao Formation ranges from 1.74 to 1.00 Ga (Lai Ke et al., 2017). Therefore, the ages of the inherited zircons (1.15–1.81 Ga, Table 1 and Fig. 5) and the  $T_{DM2}$  of magmatic zircons (1.33–2.42 Ga, mean 1.66 Ga, Table 3) in the Yangbishan granite are consistent with the ages of other zircons in the Xingdong Group. These data indicate that the peraluminous Yangbishan S-type granite formed via the partial melting of lower-crustal rocks in a reducing environment, similar to the Al-enriched paragneiss of the Dapandao Formation.

#### 6.4 Metallogenic mechanisms and sources of metallogenic elements

The trace and rare earth element contents of the scheelite from the Yangbishan deposit are similar to those of the gneissic granite, indicating that the ore-forming fluid was related to, or inherited from, the granite. We guess that the Ca in the Yangbishan deposit was probably derived from the marble of the Dapandao Formation.

Many studies have demonstrated close relationships between tungsten mineralization and S-type granites, especially highly-fractionated S-type granites (Wang Die et al., 2011; Guo et al., 2012; Feng et al., 2013; Mao et al., 2015; Guo Chunli et al., 2017; Guo Zhihua et al., 2017). As a result of the Pan-African Orogeny, massifs in northeast China were subjected to multiple continent–continent collisions, and the resultant shortening and thickening of the continental crust caused anatexis of the Precambrian metamorphic basement, yielding peraluminous magmas that were enriched with tungsten. The Yangbishan gneissic granite is a highly fractionated crustal granite similar to the W-enriched, two-mica granites of Dengfuxian in southern China, which suggests that highly fractionated crustal granite has good potential for mineralization (Cai Yang et al., 2013). Moreover, Robb (2005) suggested that the sources of S-type granites are mudstones, which may contain organic carbon. After

partial melting of the source rocks into metamorphosed mudstones, the organic carbon formed volatiles, such as  $CH_4$ , and generated a reducing environment for the entire magma system (Candela and Bouton, 1990). In such a setting, tungsten element was incompatible and had a very small partition coefficient (0.05; Robb, 2005), which means that the tungsten content increased with fractionation. In this way, a highly fractionated and reduced magma would provide suitable conditions for tungsten enrichment.

The fluoritization in the tungsten ore of the Yangbishan deposit suggests that the ore-forming fluids were enriched with fluorine. Although previous studies have shown that the transport of tungsten in a hydrothermal system is not in the form of a fluorine–chlorine complex (Wesolowski et al., 1984; Keppler and Wyllie, 1991), the presence of fluorine can make tungsten element easier to incorporate into a silicate melt (Manning, 1984; Manning and Henderson, 1984; Keppler and Wyllie, 1991). Fluorine improves the solubility of tungsten in water-rich magma (Webster, 1990; Xiong Xiaolin et al., 1998), increasing the tungsten content of the magma and delaying the separation of tungsten-bearing hydrothermal fluids from the magma (Ma Dongsheng, 2009).

Previous data have shown that elemental tungsten has siderophilic characteristics under high-temperature reducing conditions. The conclusion in this paper is that under higher temperatures, and more strongly reducing conditions, the enrichment of tungsten in the metal phases will rise (Bischoff and Palme, 1987; Wasson and Kallemeyn, 1988; Sylvester et al., 1990). This explains the enrichment of scheelite in deposits with abundant pyrrhotite in the Yangbishan deposit.

Data in this paper show that the scheelite in the Yangbishan deposit inherited most of its trace element and REE features from its host rocks, which were enriched to some degree in ore-forming material (e.g.,  $WO_4^{2-}$ ). Data on fluid inclusions in the quartz and scheelite of the Yangbishan deposit (unpublished data), including temperature measurements and analysis of gas phase compositions using laser Raman spectroscopy, indicate that the ore-forming fluids belonged to a low-salinity NaCl–H<sub>2</sub>O–CO<sub>2</sub> system at moderate–high temperatures. Liu Yingjun and Ma Dongsheng (1987) proposed that the CO<sub>2</sub> content of the ore-forming fluid is an effective indicator of tungsten mineralization, and that a high CO<sub>2</sub> concentration favors the migration of Fe<sup>2+</sup>, Mn<sup>2+</sup>, and Ca<sup>2+</sup>, as well as the stable migration of  $WO_4^{2-}$ . In addition, the metasomatism of carbonate rocks by ore-forming fluids (and the attendant fluid boiling, CO<sub>2</sub> escape, falling temperatures, rising pH values, etc.) plays an important role in the precipitation of scheelite (Wood and Samson,

2000). Wu Shenghua et al. (2014) suggested that decreasing temperatures and increasing alkalinity induced the tungsten precipitation in the Xianglushan skarn tungsten deposit. The fact that the Xianglushan deposit and the Yangbishan deposit are similar in their fluid inclusion type, gaseous composition, homogenization temperature, and ore-forming fluid salinity supports the conclusion that a decrease in temperature and an increase in alkalinity are the most important mechanisms for tungsten precipitation.

In the case of Yangbishan, the gneissic granite magma was closely associated with the skarn scheelite mineralization, which reflects the following: (i) the magma source provided a reducing environment enriched in tungsten, and this enrichment was enhanced during fractionation of the magma; (ii) the late-stage ore-forming fluid was strongly reducing and contained large amounts of fluorine and CO<sub>2</sub>, which favored the enrichment and migration of tungsten; (iii) metasomatic reactions with the tungsten-rich carbonate wall-rocks of the Dapandao Formation extracted more of the ore-forming minerals; and (iv) decreasing temperature and increasing alkalinity induced the tungsten precipitation.

In the Mesoproterozoic, the silicon- and iron-rich Dapandao Formation, which has high tungsten content, was deposited in a stable continental margin environment, where the source beds of the iron–tungsten ores were formed. These sediments probably contained some iron-rich deposits. A subsequent regional high-grade metamorphism and recrystallization event resulted in the mobilization of this sedimentary iron, which was superimposed on the original ores, causing the formation of higher-grade iron ores (Wei Lianxi, 2013). In the Cambrian, the late Pan-African orogeny resulted in the amalgamation of micro-continental blocks in northeast China due to continent–continent collisions. The shortening and thickening of the continental crust during these collisions caused anatexis of the Precambrian basement, forming tungsten-enriched peraluminous magmas. The magmas then intruded into the carbonate rocks of the Dapandao Formation, which already contained significant amounts of ore-forming elements. The interaction between the ore-bearing fluid and the carbonate rocks resulted in the formation of skarn-type tungsten ores as layers and layer-like bodies in the endo- and exo-contact zones, concentrated between the granite and the host strata. The Yangbishan iron–tungsten deposit was formed as a result of this “variant-orebody paragenesis.”

### 6.5 Tectonic setting

Previous geochronological data (Table 8) have indicated

that microcontinents in northeast China, including the Jiamusi Massif, experienced metamorphism and accompanying magmatic activity from 530 Ma to 500 Ma (Wu Fuyuan et al., 1999, 2001; Wu et al., 2007; Wilde et al., 2000, 2003; Wilde Simona et al., 2001; Xie Hangqiang et al., 2008; Wen Quanbo et al., 2008; Huang Yingcong et al., 2009; Ren Liudong et al., 2010; Zhou et al., 2010a, b; Zhou Jianbo et al., 2011; Dong Ce and Zhou Jianbo, 2012; Zhang Xingzhou et al., 2012; Bi et al., 2014; Zhao Liangliang et al., 2014). As mentioned above, the crystallization age of the Yangbishan gneissic granite is  $520.6 \pm 2.8$  Ma, which means that it is a record of early Paleozoic magmatic events. The Mashan Group in the Jiamusi Massif and the Hutou complex in the nearby Khanka Massif are not only record of early Paleozoic magmatic events but also record of metamorphic events (Song Biao et al., 1997; Wu et al., 2007; Zhou et al., 2010b). The muscovite-bearing peraluminous Yangbishan gneissic granite contains garnet and muscovite, and its crystallization temperature is 738–750°C. The granite was derived mainly from melted crust during orogenesis (Barbarin, 1999), and it has the geochemical signature of syn-collisional granite (Maniar and Piccoli, 1989), which can be related to the collisions of microcontinents taking place at this time. In the Rb–(Y + Nb), Rb–(Yb + Ta), Rb/30–Hf–Ta $\times$ 3, and Rb/30–Hf–Ta $\times$ 3 diagrams (Fig. 13a–d), the Yangbishan gneissic granite samples all plot in the syn-collisional granite field. These data suggest that, at 520 Ma, the Jiamusi Massif was in a compressional environment that resulted from continent–continent collisions.

The latest geochronological data (Table 8) suggest that Pan-African magmatic and metamorphic events were widespread in northeast China (Dong Ce and Zhou Jianbo, 2012; Zhang Xingzhou et al., 2012; Zhou Jianbo et al., 2012; Zhou and Wilde, 2013), which is a mosaic of massifs, including the Erguna, Xing'an, Songliao, Jiamusi, and Khanka massifs. The geochronological data of the gneissic granite, as well as the gneissose structures in the rocks associated with the Yangbishan tungsten mineralization, indicate that the Jiamusi Massif was in a syn-collisional orogenic setting c. 520 Ma. In addition, the presence of Lower Cambrian strata in Heilongjiang Province and the absence of Middle–Upper Cambrian strata (HBGMR, 1993) imply that, during the Middle–Late Cambrian, the massifs in northeast China underwent orogenic movements and uplift, accompanied by erosion. Ge Wenchun et al. (2007b) also proposed that the Khanka orogeny, associated with the Pan-African orogeny, took place in the late-early Cambrian and formed the basement of the Xing'an Massif, resulting in the Middle–Late Cambrian stratigraphic gap. In the early Ordovician, the

**Table 8 Geochronological data of Early Paleozoic rocks in NE China**

Sampling point	Rock tested	Test method	Test result (Ma)	Genesis of zircon	References
<b>Jiamusi Massif</b>					
Liumao	garnet granulite		502 ± 8	metamorphic	Wilde et al., 2001
Liumao	anatectic granite		502 ± 10	metamorphic	Wilde et al., 2001
Liumao	gneissic granite		498 ± 7/530-1460	metamorphic	Wilde et al., 2001
Sandaogou	sillimanite gneiss	SHRIMP zircon U-Pb	496 ± 8	metamorphic	Wilde et al., 2001
Ximashan	garnet granite		507 ± 12	metamorphic	Wilde et al., 2001
Ximashan	garnet granulite		500 ± 9/1900 ± 14	metamorphic	Wilde et al., 2001
Ximashan	sillimanite gneiss		495 ± 15/1675 ± 7	metamorphic	Wilde et al., 2001
Majiajie	granitic gneiss		560 ± 2/504 ± 2	magmatic/metamorphic	Huang Yingcong et al., 2009
		LA-ICP-MS zircon U-Pb			Huang Yingcong et al., 2009
Dapandao	granitic gneiss		506 ± 4	magmatic	Huang Yingcong et al., 2009
Shuangyashan	biotite monzonitic gneiss	Monazite CHIME	494 ± 23		Wen Quanbo et al., 2008
Boli	granitic gneiss		481 ± 23		Wen Quanbo et al., 2008
Muling	striped migmatite		490-531	metamorphic	Xie Hangqiang et al., 2008
Muling	gneissic granite	LA-ICP-MS zircon U-Pb	486 ± 3/477 ± 9	magmatic/metamorphic	Xie Hangqiang et al., 2008
Jiamusi	porphyritic granite		515 ± 8/479 ± 16	magmatic/metamorphic	Wilde et al., 2003
Sandaogou	biotite granite gneiss	SHRIMP zircon U-Pb	523 ± 8/498 ± 16	magmatic/metamorphic	Wilde et al., 2003
Ximashan	biotite plagioclase gneiss	Zircon stepped evaporation	526 ± 4	metamorphic	Song Biao et al., 1997
Yaotun	monzonitic granite		507 ± 4	magmatic	Bi et al., 2014
Yaotun	syenogranite		493 ± 3	magmatic	Bi et al., 2014
Qixingpao	monzonitic granite		506 ± 3	magmatic	Bi et al., 2014
Qixingpao	granodiorite		497 ± 8	magmatic	Bi et al., 2014
Baoshihe	syenogranite		493 ± 4	magmatic	Bi et al., 2014
Baoshihe	granodiorite		530 ± 5	magmatic	Bi et al., 2014
Baoshihe	monzonitic granite	LA-ICP-MS zircon U-Pb	488 ± 3	magmatic	Bi et al., 2014
Baoshihe	syenogranite		490 ± 3	magmatic	Bi et al., 2014
Lanfeng	syenogranite		484 ± 3	magmatic	Bi et al., 2014
Xiaochengzi	monzonitic granite		518 ± 10	magmatic	Bi et al., 2014
Yangbishan	gneissic granite		520 ± 3	magmatic	This study
Suibin	biotite monzonitic gneiss		496 ± 6	magmatic	Gao Fuhong et al., 2010
Muling	migmatitic granite		493 ± 4	magmatic	Ren Liudong et al., 2010
<b>Xingkai Massif</b>					
Hutou	sillimanite gneiss		490 ± 4	metamorphic	Zhou et al., 2010a
Hutou	garnet granite gneiss	LA-ICP-MS zircon U-Pb	522/510-500	magmatic/metamorphic	Zhou et al., 2010b
Hutou	garnet granite gneiss		515 ± 8/510-500	magmatic/metamorphic	Zhou et al., 2010b
<b>Songliao Massif</b>					
Yichun	gneissic granite	SHRIMP zircon U-Pb	508 ± 15	magmatic	Liu Jianfeng et al., 2008
Yichun	granodiorite		499 ± 1	magmatic	Liu Jianfeng et al., 2008
Yichun	biotite granite		496 ± 2	magmatic	Chen Xian et al., 2014
Yichun	monzonitic granite	LA-ICP-MS zircon U-Pb	504 ± 5	magmatic	Niu Yanhong et al., 2015
<b>Erguna Massif</b>					
Tahe	porphyritic monzonitic granite		499 ± 1	magmatic	Ge Wenchun et al., 2007a
Tahe	granodiorite		500 ± 1	magmatic	Ge Wenchun et al., 2007a
Tahe	porphyritic syenogranite	LA-ICP-MS zircon U-Pb	493 ± 5	magmatic	Ge Wenchun et al., 2005
Tahe	porphyritic syenogranite		494 ± 9	magmatic	Ge Wenchun et al., 2005
Tahe	syenogranite		480 ± 4/518 ± 7	magmatic	Ge Wenchun et al., 2005
Tahe	amphibole gabbro		490 ± 3/531 ± 19	magmatic	Ge Wenchun et al., 2005
Tahe	biotite monzonitic granite		485 ± 3/521 ± 6	magmatic	Ge Wenchun et al., 2005
Mohe	plagioclase hornblende gneiss		495 ± 2	metamorphic	Zhou et al., 2010a
Mohe	garnet sillimanite gneiss		496 ± 3	metamorphic	Zhou et al., 2010a
Mohe	biotite plagioclase gneiss	SHRIMP zircon U-Pb	496 ± 8	metamorphic	Zhou et al., 2010a
Mohe	quartz diorite		517 ± 9	magmatic	Wu Guang et al., 2005
Mohe	monzonitic granite		504 ± 8	magmatic	Wu Guang et al., 2005
<b>Xing'an Massif</b>					
Greater					
Xing'an Mountains	sillimanite garnet gneiss	SHRIMP zircon U-Pb	494 ± 2	metamorphic	Zhou et al., 2010b
Duobaoshan	granodiorite		485 ± 8	magmatic	Ge Wenchun et al., 2007b
Duobaoshan	granodiorite	LA-ICP-MS zircon U-Pb	476 ± 1	magmatic	Hao et al., 2015

Xing'an Massif began to stretch and was in the early stages of geosyncline development. Considering the minor components and chemical composition of the early Ordovician granodiorites of the Duobaoshan porphyry copper-molybdenum deposit located in the Xing'an

Massif, Wu et al. (2015) posited that these intrusions were most likely formed in a post-collision setting. Similarly, Ge Wenchun et al., (2005) suggested that the Tahe intrusive rock (480–494 Ma) in the Erguna Massif was formed in a post-orogenic environment. Based on studies

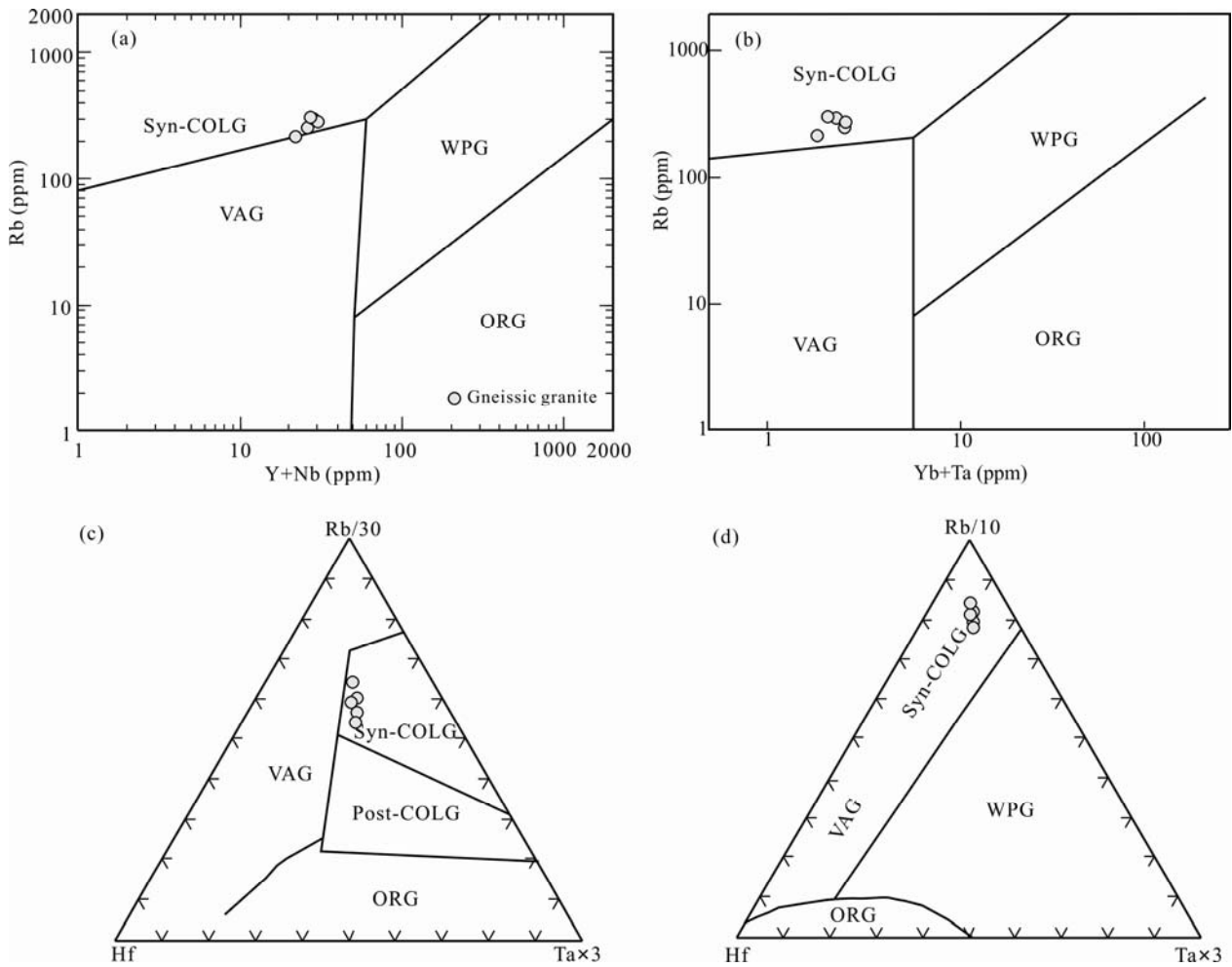


Fig. 13. Tectonic discrimination diagrams of the Yangbishan gneissic granite.

(a), Rb vs Y+Nb diagram (after Pearce et al., 1984); (b), Rb vs Yb+Ta diagram (after Pearce et al., 1984); (c), Hf vs Rb/30 vs Ta $\times$ 3 diagram (after Harris et al., 1986); (d), Hf vs Rb/10 vs Ta $\times$ 3 diagram (after Harris et al., 1986). Fields for syn-collision (COLG), post-collision, volcanic arc (VAG), within plate (WPG) and ocean ridge (ORG) granites are indicated.

of a monzonitic granite ( $508 \pm 15$  Ma), granodiorite ( $499 \pm 1$  Ma), and alkali-feldspar granite ( $471 \pm 3$  Ma) in the eastern part of the Lesser Xing'an Range, Liu Jianfeng et al. (2008) suggested that these intrusive bodies represent a structural evolution and transition from syn-collision to post-collision. All in all, the evidence indicates that from the early to the late stage of the early Paleozoic (530–470 Ma), the tectonic setting of the magmatic activity in northeast China changed from syn-collisional (compression) to post-collisional (extension) (Huang Yingcong, 2009).

The early Paleozoic Sayan–Baikal orogenic belt along the southern margin of the Siberian Plate, and the Moren, Erzin, and Naryn complexes in the Tuva–Mongolia Massif, also record magmatic and metamorphic events c. 500 Ma (Salnikova et al., 1998; Donskaya et al., 2000; Todt et al., 2001; Khain et al., 2003; Gladkochub et al., 2008). However, this metamorphic event was not recorded in the North China Craton and neighboring regions, which suggests that the tectonic history of the northeast China

massifs during the Pan-African event is closely tied to that of the Siberian Plate (Zhou et al., 2009, 2010a, b, c, 2011a, b; Zhou Jianbo et al., 2011, 2012; Zhang Xingzhou et al., 2012). All of these massifs seem to be part of the same orogenic belt that formed along the southern margin of the Siberian Craton during the late Pan-African orogeny. This inference is supported by paleontological data (Duan Jiye and An sultan, 2001). Early Paleozoic mineralization similar to that observed in Yangbishan, c. 500 Ma, has been identified in the Tuva–Mongolia Massif. Notable locations with this mineralization pattern include the Yangbishan skarn tungsten deposit, the Duobaoshan and Tongshan porphyry copper–molybdenum deposit, the Zhengguang epithermal gold deposit in northeast China (Hao et al., 2015, 2016; Wu et al., 2015), the Bozshakol porphyry copper–gold deposit in Kazakhstan, and the Taldy Bulak porphyry gold–copper deposit in Kyrgyzstan (Mao et al., 2014). This widespread magmatism and mineralization might have resulted from the Pan-African orogeny. It can be deduced, therefore, that the Jiamusi,

Khanka, Xing'an, Songliao, and Erguna massifs became amalgamated to form a Pan-African Massif in response to the Pan-African orogenic movements (Zhou et al., 2010b; Zhou Jianbo et al., 2012; Xue Mingxuan, 2012). The large Massif was subsequently broken up between 450 Ma and 300 Ma in response to the opening of the Mongolia–Okhotsk Ocean (Fig. 14; Zhou Jianbo et al., 2012; Zhou et al., 2013).

In summary, the massifs in northeast China, including the Erguna, Xing'an, Songliao, Jiamusi, and Khanka massifs, were parts of an orogenic belt that formed along the southern margin of the Siberian Craton during the late Pan-African period. Magmatic activity was dominantly related to compressional continent–continent collisions, but there was a progressive evolution and transition as the

tectonic setting shifted from syn-collisional to post-collisional between 530 Ma and 470 Ma.

## 7 Conclusions

(1) The tungsten mineralization in the Yangbishan deposit is skarn-type. The crystallization age of the gneissic granite associated with scheelite mineralization is  $520.6 \pm 2.8$  Ma, indicating that the tungsten mineralization occurred during the earliest Paleozoic. This means that the Yangbishan is the oldest tungsten deposit discovered, to date, in northeast China. These data imply that undiscovered Paleozoic tungsten deposits may exist in the eastern section of the CAOB.

(2) The scheelite in the Yangbishan deposit was

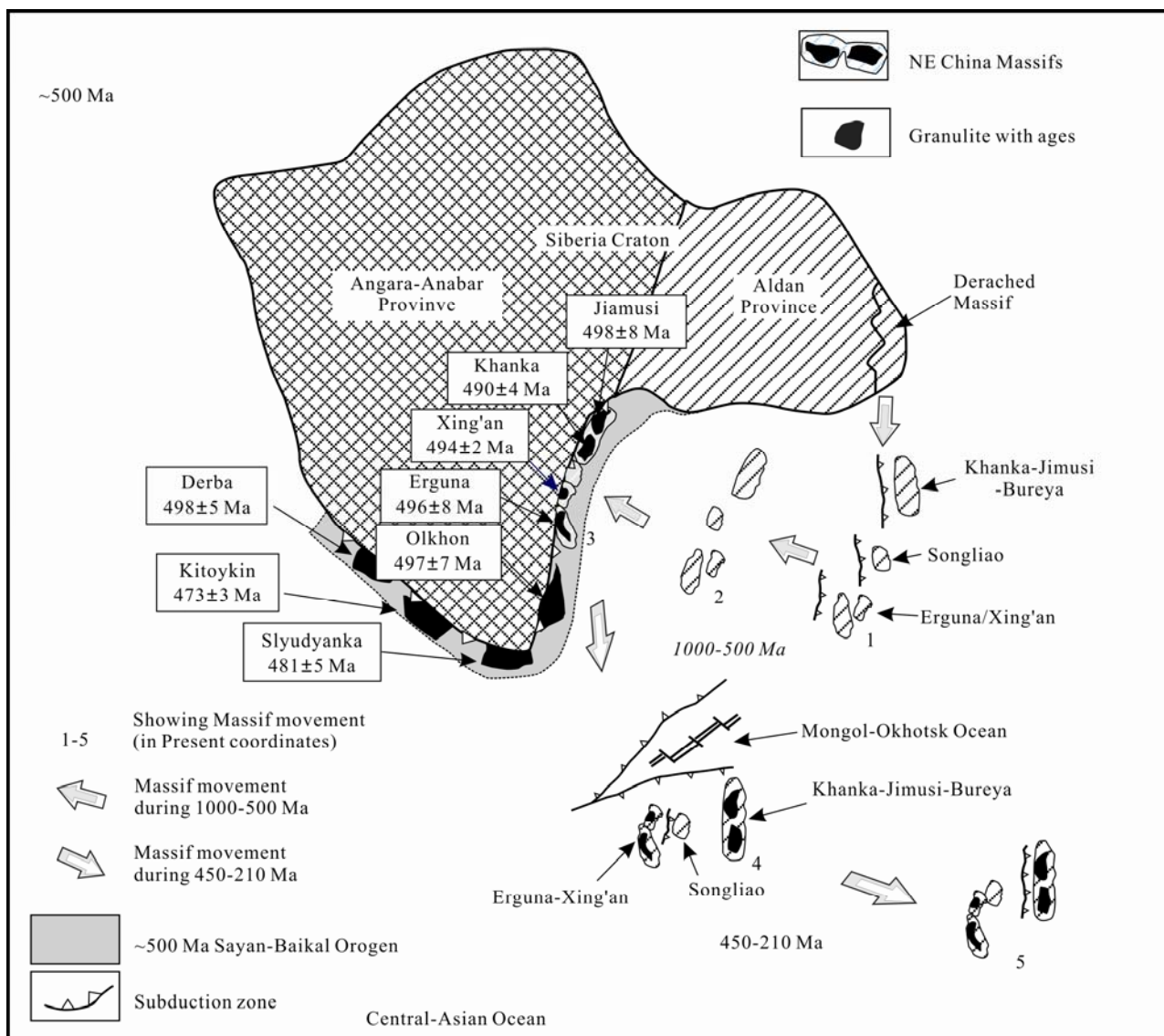


Fig. 14. A cartoon model showing possible source region and subsequent drift history of the NE China blocks during 1000–500 Ma and 450–210 Ma (modified from Salnikova et al., 1998; Gladkochub et al., 2008; Zhou et al., 2010c).

precipitated in a reducing environment and inherited its REE features of the ore-forming fluids from which it formed. REE<sup>3+</sup> replaced Ca<sup>2+</sup> and entered scheelite by substitution. The ore sources for the tungsten mineralization probably formed via interactions between magmatic hydrothermal solutions and the surrounding host rocks.

(3) The Yangbishan gneissic granite is a highly fractionated S-type granite, and its source rock was originally shale that formed in a reducing environment and contained organic material. Following metamorphism, the source rock was similar to the Al-enriched paragneisses of the Dapandao Formation of the Xingdong Group. The partial melting in the lower crust led to magmas that experienced a high degree of fractionation, producing strongly reduced, fluorine- and CO<sub>2</sub>-rich ore-forming fluids. These factors provided favorable metallogenic conditions for the skarn scheelite mineralization in the Yangbishan deposit.

(4) Massifs in northeast China, including the Erguna, Xing'an, Songliao, Jiamusi, and Khanka massifs, were parts of an orogenic belt that formed along the southern margin of the Siberian Craton during the late Pan-African orogeny. The magmatic activity and associated metallogenic events in northeast China took place in a tectonic setting that evolved over the period of 530 Ma to 470 Ma, transitioning from compression during the amalgamation of microcontinents to extension in the post-collisional stage.

## Acknowledgments

This work was supported by the National Key R&D Program of China (2017YFC0601304), the National Basic Research Program of China (also called 973 Program) (No. 2013CB429802) and the National Natural Science Foundation of China (NSFC) (No. 41272094). We thank the Reviewers for their comments that helped improve the manuscript.

Manuscript received Dec. 21, 2016  
accepted Sept. 13, 2017  
edited by Fei Hongcai

## References

- Barbarin, B., 1999. A review of the relationships between granitoid types, their origins and their geodynamic environments. *Lithos*, 46(3): 605–626.
- Bea, F., Montero, P., Garuti, G., and Zacharini, F., 1997. Pressure-dependence of rare earth element distribution in amphibolite- and granulite-grade garnets. A LA-ICP-MS study. *Geostandards & Geostandards Newsletters*, 21(2): 253–270.
- Bi, J.H., Ge, W.C., Yang, H., Zhao, G.C., Yu, J.J., Zhang, Y.L., Wang, Z.H., and Tian, D.X., 2014. Petrogenesis and tectonic implications of early Paleozoic granitic magmatism in the Jiamusi Massif, NE China: Geochronological, geochemical and Hf isotopic evidence. *Journal of Asian Earth Science*, 96: 308–331.
- Bischoff, A., and Palme, H., 1987. Composition and mineralogy of refractory metal-rich assemblages from a Ca, Al-rich inclusion in the Allende meteorite. *Geochimica et Cosmochimica Acta*, 51(10): 2733–2748.
- Blichert-Toft, J., and Albarede, F., 1997. The Lu–Hf isotope geochemistry of shergottites and the evolution of the Martian mantle–crust system. *Earth and Planetary Science Letters*, 154(1–4): 243–258.
- Boyd, F.R., Pearson, D.G., Hoal, K.O., Hoal, B.G., Nixon, P.H., Kingston, M.J., and Mertzman, S.A., 2004. Garnet lherzolites from Louwrensia, Namibia: bulk composition and P/T relations. *Lithos*, 77(1–4): 573–592.
- Boynton, W.V., 1984. Cosmochemistry of the rare earth elements: meteoric studies. *Rare Earth Element Geochemistry*, 2(2): 63–114.
- Brugger, J., Lahaye, Y., Costa, S., Lambert, D., and Bateman, R., 2000. Inhomogeneous distribution of REE in scheelite and dynamics of Archaean hydrothermal systems (Mt. Charlotte and Drysdale gold deposits, Western Australia). *Contributions to Mineralogy Petrology*, 139(3): 251–264.
- Brugger, J., Mass, R., Lahaye, Y., Mcrae, C., Ghaderi, M., Costa, S., Lambert, D., Bateman, R., and Prince, K., 2002. Origins of Nd–Sr–Pb isotopic variations in single scheelite grains from Archaean gold deposits, Western Australia. *Chemical Geology*, 182(2): 203–225.
- Cai Yang, Lu Jianjun, Ma Dongsheng, Huang Hui and Zhang Huaifeng, 2013. Chronology and geochemical characteristics of Late Indosinian Dengfuxian two–mica granite in eastern Hunan Province, China, and its significance. *Acta Petrologica Sinica*, 29(12): 4215–4231 (in Chinese with English abstract).
- Candela, P.A., and Bouton, S.L., 1990. The influence of oxygen fugacity on tungsten and molybdenum partitioning between silicate melts and ilmenite. *Economic Geology*, 85(3): 633–640.
- Chappell, B.W., and White, A.J.R., 1992. I- and S-type granites in the Lachlan Fold Belt. *Transactions of the Royal Society of Edinburgh: Earth Sciences*, 83(1–2): 1–26.
- Chen Runsheng, 2013. *Geology, geochemistry and metallogenesis of the Shangfang tungsten deposit in Jianou county, Northern Fujian Province, SE China*. Wuhan: China University of Geosciences (Ph. D thesis): 1–168 (in Chinese with English abstract).
- Chen Xian, Liu Jiajun, Zhang Qibin, Yang Zenghai, Yang Longbo and Wu Jie, 2014. Characteristics of Hf isotopes and zircon U–Pb ages of granites in the Cuihongshan iron polymetallic deposit, Heilongjiang and their geological implication. *Bulletin of Mineralogy, Petrology and Geochemistry*, 33(5): 636–644 (in Chinese with English abstract).
- Chu, N.C., Taylor, R.N., Chavagnac, V., Nesbitt, R.W., Boella, R.M., Milton, J.A., German, C.R., Bayon, G., and Burton, K., 2002. Hf isotope ratio analysis using multi-collector inductively coupled plasma mass spectrometry: an evaluation of isobaric interference corrections. *Journal of Analytical Atomic Spectrometry*, 17(12): 1567–1574.

- Corfu, F., Hanchar, J.M., Hoskin, P.W.O., and Kinny, P., 2003. Atlas of zircon textures. *Review in Mineralogy and Geochemistry*, 53 (1): 469–495.
- Dong Ce and Zhou Jianbo, 2012. Geochemistry of ~500 Ma Pan–African khondalite series in west of NE China and its tectonic implications. *Acta Petrologica Sinica*, 28(9): 2866–2878 (in Chinese with English abstract).
- Donskaya, T.V., Sklyarov, E.V., Gladkochub, D.P., and Berezhnaya, N.G., 2000. The Baikal collisional metamorphic belt. *Doklady Earth Sciences*, 374(7): 1075–1079.
- Dostal, J., Kontak, D.J., and Chatterjee, A., 2009. Trace element geochemistry of scheelite and rutile from metaturbidite-hosted quartz vein gold deposits, Meguma Terrane, Nova Scotia, Canada: Genetic implications. *Mineralogy and Petrology*, 97(1–2): 95–109.
- Duan Jiye and An Sulan, 2001. Early Cambrian Siberian Eauna from Yichun of Heilongjiang Province. *Acta Palaeontologica Sinica*, 40(3): 362–370 (in Chinese with English abstract).
- Eggins, S.M., Kinsley, L.P.J., and Shelley, J.M.M., 1998. Deposition elemental fractionation processes during atmospheric pressure laser sampling for analysis by ICP–MS. *Applied Surface Science*, 127–129: 278–286.
- Eichhorn, R., Höll, R., Jagout, E., and Schärer, U., 1997. Dating scheelite stages: A strontium, neodymium, lead approach from the Felhertal tungsten deposit, Central Alps, Austria. *Geochimica Et Cosmochimica Acta*, 61(23): 5005–5022.
- Elhlou, S., Belousova, E., Griffin, W.L., Pearson, N.J., and O'Reilly, S.Y., 2006. Trace element and isotopic composition of GJ–red zircon standard by laser ablation. *Geochimica Et Cosmochimica Acta*, 70(18): A158.
- Feng, J.R., Mao, J.W., and Pei, R.F., 2013. Ages and geochemistry of Laojunshan granites in southeastern Yunnan, China: implications for W–Sn polymetallic ore deposits. *Mineralogy and Petrology*, 107(4): 573–589.
- Gao Fuhong, Wang Feng, Cao Huahua, Zheng Yuhang and Liu Jun, 2010. Zircon U–Pb age of the basement granite from Suibin depression in Sanjiang basin and its tectonic implications. *Journal of Jilin University: Earth Science Edition*, 40(4): 955–960 (in Chinese with English abstract).
- Gao Shan, Luo Tingchuan, Zhang Benren, Zhang Hongfei, Han Yinwen, Zhao Zhidan and Kern Hartmut, 1999. Structure and composition of the continental crust in East China. *Sciences in China (Series D)*, 29(3): 204–213 (in Chinese).
- Ge Wenchun, Wu Fuyuan, Zhou Changyong and Rahman A.A.Abodel, 2005. Emplacement age of the Tahe granite and its constraints on the tectonic nature of the Ergun block in the northern part of the Da Hinggan Range. *Chinese Science Bulletin*, 20(12): 2097–2105 (in Chinese).
- Ge Wenchun, Sui Zhenmin, Wu Fuyuan, Zhang Jiheng, Xu Xuechun and Cheng Ruiyu, 2007a. Zircon U–Pb ages, Hf isotopic characteristics and their implications of the Early Paleozoic granites in the northeastern Da Hinggan Mts., northeastern China. *Acta Petrologica Sinica*, 23(2): 423–440 (in Chinese with English abstract).
- Ge Wenchun, Wu Fuyuan, Zhou Changyong and Zhang Jiheng, 2007b. Porphyry Cu–Mo deposits in the eastern Xing'an–Mongolian Orogenic Belt: Mineralization ages and their geodynamic implications. *Chinese Science Bulletin*, 52(20): 3416–3427 (in Chinese).
- Ghaderi, M., Palin, J.M., Campbell, I.H., and Sylvester, P.J., 1999. Rare earth element systematics in scheelite from hydrothermal gold deposits in the Kalgoorlie–Norseman region, Western Australia. *Economic Geology*, 94(3): 423–437.
- Gladkochub, D.P., Donskaya, T.V., Wingate, M.T.D., Poller, U., Kröner, A., Fedorovsky, V.S., Mazukabov, A.M., Todt, W., and Pisarevsky, S.A., 2008. Petrology, geochronology, and tectonic implications of ca. 500Ma metamorphic and igneous rocks along the northern margin of the Central Asian Orogen (Olkhon terrane, Lake Baikal, Siberia). *Journal of the Geological Society of London*, 165(9): 235–246.
- Grauch, R.I., 1989. Rare earth elements in metamorphic rocks. *Reviews in Mineralogy*, 21(8): 147–167.
- Guo Chunli, Zeng Lingsen, Gao Li'e, Su Hongzhong, Ma Xinghua and Yin Bing, 2017. Highly fractionated granitic minerals and whole-rock geochemistry prospecting markers in Hetian, Fujian Province. *Acta Geologica Sinica*, 91(8): 1796–1817 (in Chinese with English abstract).
- Guo Zhihua, Zhang Baolin, Dang Yongqi, Guo Bowei, Gao Lei, Hou Jinliang and Zhang Lichun, 2017. Zircon U–Pb ages and its significance of syenite porphyry in Bayinsuhetu tungsten deposit, Mongolia. *Geological Review*, 63(5): 1378–1390 (in Chinese with English abstract).
- Guo, C.L., Chen, Y.C., Zeng, Z.L., and Lou, F.S., 2012. Petrogenesis of the Xihuashan granites in southeastern China: Constraints from geochemistry and in-situ analyses of zircon U–Pb–Hf–O isotopes. *Lithos*, 148(5S): 209–227.
- Guo, Z.J., Li, J.W., Xu, X.Y., Song, Z.Y., Dong, X.Z., Tian, J., Yang, Y.C., She, H.Q., Xiang, A.P., and Kang, Y.J., 2016. Sm–Nd dating and REE composition of scheelite for the Honghuaerji scheelite deposit, Inner Mongolia, Northeast China. *Lithos*, 261: 307–321.
- Hao Yujie, Ren Yunsheng, Zou Xintong, Chen Cong, Hou Zhaoshuo and Qu Wenjun, 2013. Re–Os isotopic dating of the molybdenite from the Cuihongshan W–Mo polymetallic deposit in Heilongjiang Province and its geological significance. *Journal of Jilin University (Earth Science Edition)*, 43(6): 1840–1850 (in Chinese with English abstract).
- Hao, Y.J., Ren, Y.S., Duan, M.X., Tong, K.Y., Chen, C., Yang, Q., and Li, C., 2015. Metallogenic events and tectonic setting of the Duobaoshan ore field in Heilongjiang Province, NE China. *Journal of Asian Earth Sciences*, 97: 442–458.
- Hao, Y.J., Ren, Y.S., Duan, M.X., Zhao, X., and Yang, Q., 2016. Mineralization time and tectonic setting of the Zhengguang Au deposit in the Duobaoshan ore field, Heilongjiang Province, NE China. *Arabian Journal of Geosciences*, 9(15): 655.
- Harris, N.B.W., Pearce, J.A., and Tindle, A.G., 1986. Geochemical characteristics of collision–zone magmatism. *Geological Society London Special Publications*, 19(5): 67–81.
- Hazarika, P., Mishra, B., and Pruseth, K.L., 2016. Scheelite, apatite, calcite and tourmaline compositions from the late Archean Hutti orogenic gold deposit: Implications for analogous two stage ore fluids. *Ore Geology Review*, 72: 989–1003.
- HBGMR (Heilongjiang Bureau of Geology and Mineral Resources), 1993. *Regional Geology of Heilongjiang Province*. Beijing: Geological Publishing House, 734 (in Chinese with English abstract).
- Henderson, P., 1985. Crystal chemistry and geochemistry of some mineral crystal. *Geology Geochemistry Supplement*, 1–

- 4.
- Hou Kejun, Li Yanhe, Zou Tianren, Qu Xiaoming, Shi Yuruo and Xie Guiqing, 2007. Laser ablation–MC–ICP–MS technique for Hf isotope microanalysis of zircon and its geological applications. *Acta Petrologica Sinica*, 23(10): 2595–2604 (in Chinese with English abstract).
- Hu Zhenghua, 2015. *The formation conditions and metallogenic regularity of Zhuxi tungsten polymetallic deposit in northeast of Jiangxi Province*. Chengdu: Chengdu University of Technology (Ph.D thesis): 1–195 (in Chinese with English abstract).
- Huang Yingcong, 2009. *Paleozoic metamorphism and tectonic evolution of Jiamusi Block*. Changchun: Jilin University (Ph.D thesis): 1–145 (in Chinese with English abstract).
- Huang Yingcong, Zhang Xingzhou, Zhang Hongbin, Xiong Xiaosong, Liu Changlin and Zhao Liangliang, 2009. Geochemical characteristics and sedimentation age of the Majiajie Group in eastern Heilongjiang Province, China. *Acta Geologica Sinica*, 83(2): 295–303 (in Chinese with English abstract).
- Jackson, S.E., Pearson, N.J., Griffin, W.L., and Belousova, E.A., 2004. The application of laser ablation–inductively coupled plasma–mass spectrometry to in situ U–Pb zircon geochronology. *Chemical Geology*, 211(1): 47–69.
- Jiang, S.H., Bagas, L., Hu, P., Han, N., Chen, C.L., Liu, Y., and Kang, H., 2016. Zircon U–Pb ages and Sr–Nd–Hf isotopes of the highly fractionated granite with tetrad REE patterns in the Shamai tungsten deposit in eastern Inner Mongolia, China: Implications for the timing of mineralization and ore genesis. *Lithos*, 261: 332–339.
- Keppler, H., and Wyllie, P.J., 1991. Partitioning of Cu, Sn, Mo, W, U, and Th between melt and aqueous fluid in the systems haplogranite–H<sub>2</sub>O–HCl and haplogranite–H<sub>2</sub>O–HF. *Contributions to Mineralogy and Petrology*, 109(2): 139–150.
- Khain, E.V., Bibikova, E.V., Salnikova, E.B., Kröner, A., Gibsher, A.S., Dodenko, A.S., Degtyarev, K.E., and Fedotova, A.A., 2003. The Palaeo–Asian Ocean in the Neoproterozoic and Early Palaeozoic: new geochronologic data and Palaeotectonic reconstructions. *Precambrian Research*, 12 (1–4): 329–358.
- King, P.L., White, A.J.R., Chappell, B.W., and Allen, C.M., 1997. Characterization and origin of aluminous A–type granite from the Lachlan fold belt, Southeastern Australia. *Journal of Petrology*, 38(3): 371–391.
- Lai Ke, Ren Yunsheng, Hao Yujie, Sun Qi, Liu Jun and Li Junying, 2017. Formation age and geological significance of Yangbishan BIF type iron deposit in Jiamusi area, Heilongjiang Province. *Global Geology*, 36(2): 495–506 (in Chinese with English abstract).
- Li Junjian, Fu Chao, Tang Wenlong, Li Huimin, Lin Yuanxian, Zhang Tong, Wang Shouguang, Zhao Zelin, Dang Zhicai and Zhao Lijun, 2016. The metallogenic age of the Shamai wolframite deposit in Dong Ujimqin Banner, Inner Mongolia. *Geological Bulletin of China*, 35(4): 524–530 (in Chinese with English abstract).
- LI Yixin, 2012. *The study on ore genesis and metallogenic geological model of Laozuoshan gold deposit in Heilongjiang Province*. Changchun: Jilin University (M.S. thesis): 1–67 (in Chinese with English abstract).
- Liu Jianfeng, Chi Xiaoguo, Dong Chunyan, Zhao Zhi, Li Guangrong and Zhao Yuandong, 2008. Discovery of Early Paleozoic granites in the eastern Xiao Hinggan Mountains, northeastern China and their tectonic significance. *Geological Bulletin of China*, 27(4): 534–544 (in Chinese with English abstract).
- Liu Yingjun and Ma Dongsheng, 1987. *Geochemistry of Tungsten*. Beijing: Science Press, 232 (in Chinese).
- Liu Yingjun, Li Zhaolin and Ma Dongsheng, 1982. The geochemical studies of tungsten built in South China. *Science in China (Series B)*, 10: 939–950 (in Chinese).
- Liu Yu, 2013. *The geological characteristics and prospecting direction of Gongpengzi Cu–Zn–W deposit in Heilongjiang Province*. Changchun: Jilin University (M.S. thesis): 1–55 (in Chinese with English abstract).
- Liu, J., Mao, J.W., Wu, G., Wang, F., Luo, D.F., and Hu, Y.Q., 2015. Geochemical signature of the granitoids in the Chalukou giant porphyry Mo deposit in the Heilongjiang Province, NE China. *Ore Geology Reviews*, 64(1): 35–52.
- Liu, Y.S., Hu, Z.C., Gao, S., Gunther, D., Xu, J., Gao, C.G., and Chen, H.H., 2008. In situ analysis of major and trace elements of anhydrous minerals by LA–ICP–MS without applying an internal standard. *Chemical Geology*, 257(1–2): 34–43.
- Ludwig, K.R., 2003. Isoplot 3.09–A Geochronological Toolkit for Microsoft Excel. *Berkeley Geochronology Center Special Publication*: 1–4.
- Ma Dongsheng, 2009. Progress in research on geochemistry of tungsten. *Geological Journal of China Universities*, 15 (1): 19–34 (in Chinese with English abstract).
- Maniar, P.D., and Piccoli, P.M., 1989. Tectonic discrimination of granitoids. *Geological Society of America Bulletin*, 101(5): 635–643.
- Manning, D.A.C., 1984. Volatile control of tungsten partitioning in granitic melt–vapour systems. *Transactions of the Institute of Mining and Metallurgy*, 93: B185–B189.
- Manning, D.A.C., and Henderson, P., 1984. The behaviour of tungsten in granitic melt–vapour systems. *Contributions to Mineralogy and Petrology*, 86(3): 286–293.
- Mao, J.W., Pirajno, F., Lehmann, B., Luo, M.C., and Berzina A., 2014. Distribution of porphyry deposits in the Eurasian continent and their corresponding tectonic settings. *Journal of Asian Earth Sciences*, 79(2): 576–584.
- Mao, Z.H., Mao, J.W., Deng, J., Zhang, F., Meng, X.Y., Xiong, B.K., Xiang, X.K., and Luo, X.H., 2015. Geochronology and geochemistry of granitoids related to the giant Dahutang tungsten deposit, middle Yangtze River region, China: Implications for petrogenesis, geodynamic setting, and mineralization. *Gondwana Research*, 28(2): 816–836.
- McDonough, W.F., and Sun, S.S., 1995. The composition of the earth. *Chemical Geology*, 120(3–4): 223–253.
- Miller, C.F., Mcdowell, S.M., and Mapes, R.W., 2003. Hot and cold granites? Implications of zircon saturation temperatures and preservation of inheritance. *Geology*, 31(6): 529–532.
- Müller, D., and Groves, D.I., 1998. Potassic igneous rocks and associated gold–copper mineralization. *Journal of Geochemical Exploration*, 60(2–3): 249–251.
- Ouyang, H.G., Mao, J.W., Santosh, M., Zhou, J., Zhou, Z.H., Wu, Y., and Hou, L., 2013. Geodynamic setting of Mesozoic magmatism in NE China and surrounding regions: Perspectives from spatio-temporal distribution patterns of ore deposits. *Journal of Asian Earth Sciences*, 78(12): 222–236.
- Patchett, P.J., White, W.M., Feldmann, H., Kielinczuk, S., and Hofmann, A.W., 1984. Hafnium/rare earth element

- fractionation in the sedimentary system and crustal recycling into the Earth's mantle. *Earth and Planetary Science Letters*, 69(2): 365–378.
- Pearce, J.A., Harris, N.B.W., and Tindle, A.G., 1984. Trace element discrimination diagrams for the tectonic interpretation of granitic rocks. *Journal of Petrology*, 25(4): 956–983.
- Peng Jiantang, Zhang Dongliang, Hu Ruizhong, Wu Mengjun, Liu Xiaoming, Qi Liang and Yu Youguang, 2010. Inhomogeneous distribution of rare earth elements (REEs) in Scheelite from the Zhazixi W–Sb Deposit, Western Hunan and its geological implications. *Geological Review*, 56(6): 810–819 (in Chinese with English abstract).
- Raimbault, L., Baumer, A., Dubru, M., Benkerrou, C., Croze, V., and Zahm, A., 1993. REE fractionation between scheelite and apatite in hydrothermal conditions. *American Mineralogist*, 78 (11): 1275–1285.
- Ren Liudong, Wang Yanbin, Yang Chonghui, Han Juan, Xie Hangqiang and Li Linshan, 2010. Metamorphism, migmatization and granites of the Mashan Complex in Heilongjiang Province, Northeast China. *Acta Petrologica Sinica*, 26(7): 2005–2014 (in Chinese with English abstract).
- Ren Yunsheng, Ju Nan, Zhao Hualei, Wang Hui, Lu Xiuquan and Wu Changzhi, 2011. Geological characteristics and fluid inclusions of Wudaogou Lode scheelite deposit in eastern Yanbian, Jilin Province. *Journal of Jilin University: Earth Science Edition*, 41(6): 1736–1744 (in Chinese with English abstract).
- Ren Yunsheng, Zhao Hualei, Lei En, Wang Hui, Ju Nan and Wu Changzhi, 2010a. Trace element and rare earth element geochemistry of the scheelite and ore genesis of the Yangjiangou large scheelite deposit in Yanbian area, northeastern China. *Acta Petrologica Sinica*, 26(12): 3720–3726 (in Chinese with English abstract).
- Ren Yunsheng, Niu Junping, Lei En, Wang Hui and Wang Xi, 2010b. Geological geochemical characteristics and metallogenesis of Sanjiazi scheelite deposit in Siping area, Jilin Province. *Journal of Jilin University (Earth Science Edition)*, 40(2): 314–320 (in Chinese with English abstract).
- Robb, L., 2005. *Introduction to Ore-Forming Processes*. Oxford: Blackwell Publishing Company, 386.
- Salnikova, E.B., Sergeev, S.A., Kotov, A.B., Yakovleva, S.Z., Steiger, L.Z., Reznitskiy, E.P., and Vasil'ev, E.P., 1998. U–Pb zircon dating of granulite metamorphism in the Sludyanskiy complex, Eastern Siberia. *Gondwana Research*, 1(2): 195–205.
- Samuel, A.B., and Mark, D.S., 2003. High-precision U–Pb zircon geochronology and the stratigraphic record. *Reviews in Mineralogy and Geochemistry*, 53(1): 305–326.
- Scherer, E., Munker, C., and Mezger, K., 2001. Calibration of the lutetium–hafnium clock. *Science*, 293(5530): 683–687.
- Simon, E.J., Norman, J.P., William, L.G., and Elena, A.B., 2004. The application of laser ablation–inductively coupled plasma–mass spectrometry to in situ U–Pb zircon geochronology. *Chemical Geology*, 211(1): 47–69.
- Song Biao, Li Jinyi, Niu Baogui and Xu Wenxi, 1997. Single-grain zircon ages and its implications in biotite–plagioclase gneiss in Mashan Group in the eastern Heilongjiang. *Acta Geoscientia Sinica*, 18(3): 306–312 (in Chinese with English abstract).
- Song Biao, Zhang Yuhai and Liu Dunyi, 2002. Introduction to the naissance of SHRIMP and its contribution to isotope geology. *Journal of Chinese Mass Spectrometry Society*, 23 (1): 58–62 (in Chinese with English abstract).
- Song, G.X., Qin, K.Z., Li, G.M., Evans, N.J., and Chen, L., 2014. Scheelite elemental and isotopic signatures: Implications for the genesis of skarn-type W–Mo deposits in the Chizhou Area, Anhui Province, Eastern China. *American Mineralogist*, 99(2–3): 303–317.
- Streckeisen, A. 1976. To each plutonic rock its proper name. *Earth-Science Reviews*, 12(1): 1–33.
- Sun, S.S., and McDonough, W.F., 1989. Chemical and isotopic systematics of oceanic basalts: implications for mantle composition and processes. *Geological Society of Special Publications*, 42(1): 313–345.
- Sun Zhenjun, Sun Guosheng, Yu Henan, Tian Yi, Liu Shanli, Xiang Zhu, Meng Jian, Xue Huaiyu and Lu Lina, 2015. Geochronology and geochemical characteristics of intrusion in the Jinchangliang gold deposit, Inner Mongolia and their tectonic significance. *Acta Geologica Sinica (English Edition)*, 89(6): 1947–1962.
- Sylvester, P.J., 1998. Post-collisional strongly peraluminous granites. *Lithos*, 45(1–4): 29–44.
- Sylvester, P.J., and Ghaderi, M., 1997. Trace element analysis of scheelite by excimer laser ablation inductively coupled plasma mass spectrometry (ELA–ICP–MS) using a synthetic silicate glass standard. *Chemical Geology*, 141(1–4): 49–65.
- Sylvester, P.J., Ward, B.J., Grossman, L., and Hutcheon, I.D., 1990. Chemical compositions of siderophile element-rich opaque assemblages in an Allende inclusion. *Geochimica Et Cosmochimica Acta*, 54(12): 3491–3508.
- Tan Chengyin, 2009. *General characteristics of the tectonic–metallogenic systems of main ore deposits in Heilongjiang Province, Northeast China*. Beijing: China University of Geosciences (Ph.D thesis): 1–248 (in Chinese with English abstract).
- Taylor, S.R., and McLennan, S.M., 1985. *The continental crust: its composition and evolution*. Oxford: Blackwell Scientific Publish, 312.
- Todt, W., Bibikova, E.V., and Nutman, A., 2001. Age of Palaeozoic granites and metamorphism in the Tuvino–Mongolian Massif of the Central Asian Mobile Belt: loss of a Precambrian Microcontinent. *Precambrian Research*, 110(1): 143–164.
- Wang Die, Lu Huanzhang and Bi Xianwu, 2011. Comparison of characteristics of ore forming fluids between quartz–vein tungsten deposits and porphyry copper deposits associated with granitic rocks. *Earth Science Frontiers*, 18(5): 121–131 (in Chinese with English abstract).
- Wasson, J.T., and Kallemeyn, G.W., 1988. Compositions of chondrites. *Philosophical Transactions of the Royal Society of London*, 325: 535–544.
- Watson, E.B., and Harrison, T.M., 1983. Zircon saturation revisited: Temperature and composition effects in a variety of crustal magma types. *Earth and Planetary Science Letters*, 64 (2): 295–304.
- Webster, J.D., 1990. Partitioning of F between H<sub>2</sub>O and CO<sub>2</sub> fluids and topaz rhyolite melt. *Contributions to Mineralogy and Petrology*, 104 (4): 424–438.
- Wedepohl, K.H., 1995. The compositions of the continental crust. *Geochimica Et Cosmochimica Acta*, 59(7): 1217–1232.
- Wei Lianxi, 2013. *Study on metallogenic regularity and quantitative prediction of nonferrous metals and precious*

- metals in Heilongjiang Province*. Changchun: Jilin University (Ph.D thesis): 1–192 (in Chinese with English abstract).
- Wen Quanbo, Liu Yongjiang, Li Weiming, Han Guoqing and Ding ling, 2008. Monazite age and its geological significance of granitoid gneiss in the Jiamusi Massif. *Journal of Jilin University* (Earth Science Edition), 38(2): 187–193 (in Chinese with English abstract).
- Wesolowski, D., Drummond, S.E., Mesmer, R.E., and Ohmoto, H., 1984. Hydrolysis equilibria of tungsten (VI) in aqueous sodium chloride solutions to 300 °C. *Inorganic Chemistry*, 23 (8): 1120–1132.
- Whalen, J.B., Currie, K.L., and Chappell, B.W., 1987. A-type granites: Geochemical characteristics, discrimination and petrogenesis. *Contributions to Mineralogy and Petrology*, 95 (4): 407–419.
- Wiedenbeck, M., Alle, P., Corfu, F., Griffin, W.L., Meier, M., Oberli, F., Vonquadt, A., Roddick, J.C., and Spiegel, W., 1995. Three natural zircon standards for U–Th–Pb, Lu–Hf, trace–element and REE analyses. *Geostandards and Geostandards Newsletter*, 19(1): 1–23.
- Wilde, S.A., Wu Fuyuan and Zhang Xingzhou, 2001. The Mashan complex: SHRIMP U–Pb zircon evidence for a late Pan–African metamorphic event in NE China and its implication for global continental reconstructions. *Geochimica*, 30(1): 35–50 (in Chinese with English abstract).
- Wilde, S.A., Wu, F.Y., and Zhang, X.Z., 2003. Late Pan–African magmatism in northeastern China: SHRIMP U–Pb zircon evidence from granitoids in the Jiamusi Massif. *Precambrian Research*, 122(1–4): 311–327.
- Wilde, S.A., Zhang, X.Z., and Wu, F.Y., 2000. Extension of a newly identified 500 Ma metamorphic terrane in North East China: further U–Pb SHRIMP dating of the Mashan Complex, Heilongjiang Province, China. *Tectonophysics*, 328(1–2): 115–130.
- Wood, S.A., and Samson, I.M., 2000. The hydrothermal geochemistry of tungsten in granitoid environments: I. Relative solubilities of ferberite and scheelite as a function of T, p, PH, and m (NaCl). *Economic Geology*, 95(1): 143–182.
- Wu Fuyuan, Sun Deyou and Lin Qiang, 1999. Petrogenesis of the Phanerozoic granites and crustal growth in Northeast China. *Acta Petrologica Sinica*, 15(2): 181–189 (in Chinese with English abstract).
- Wu Fuyuan, Wilde, S. and Sun Deyou, 2001. Zircon SHRIMP U–Pb ages of gneissic granites in Jiamusi massif, northeastern China. *Acta Petrologica Sinica*, 17(3): 443–452 (in Chinese with English abstract).
- Wu, F.Y., Yang, J.H., Lo, C.H., Wilde, S.M., Sun, D.Y., and Jahn, B.M., 2007. The Heilongjiang Group: A Jurassic accretionary complex in the Jiamusi Massif at the western Pacific margin of northeastern China. *Island Arc*, 16: 156–172.
- Wu Guang, Sun Fengyue, Zhao Caisheng, Li Zhitong, Zhao Ailin, Pang Qingbang and Li Guangyuan, 2005. Discovery of the Early Paleozoic post-collisional granites in northern margin of the Ergun massif and its geological significance. *Chinese Science Bulletin*, 50(23): 2733–2743.
- Wu, G., Chen, Y.C., Sun, F.Y., Liu, J., Wang, G.R., and Xu, B., 2015. Geochronology, geochemistry, and Sr–Nd–Hf isotopes of early Paleozoic igneous rocks in the Duobaoshan area, NE China, and their geological significance. *Journal of Asian Earth Sciences*, 97: 229–250.
- Wu Shenghua, Wang Xudong and Xiong Bikang, 2014. Fluid inclusion studies of the Xianglushan skarn tungsten deposit, Jiangxi Province, China. *Acta Petrologica Sinica*, 30(1): 178–188 (in Chinese with English abstract).
- Xiang Anping, Wang Yajun, Qin Dajun, She Hongquan, Han Zengguang, Guan Jidong and Kang Yonglian, 2014. Metallogenic and diagenetic age of Honghuaerji tungsten polymetallic deposit in Inner Mongolia. *Mineral Deposits*, 33 (2): 428–439 (in Chinese with English abstract).
- Xie Hangqiang, Miao Laicheng, Chen Fukun, Zhang Fuqin and Liu Dunyi, 2008. Characteristics of the “Mashan Group” and zircon SHRIMP U–Pb dating of granite in Muling area, southeastern Heilongjiang Province, China: constraint on crustal evolution of the southernmost of Jiamusi Massif. *Geological Bulletin of China*, 27(12): 2127–2137 (in Chinese with English abstract).
- Xiong Dexin, Sun Xiaoming, Shi Guiyong, Wang Shengwei, Gao Jianfeng and Xue Ting, 2006. Trace elements, rare earth elements (REE) and Nd–Sr isotopic compositions in scheelites and their implications for the mineralization in Daping gold mine in Yunnan Province, China. *Acta Petrologica Sinica*, 22 (3): 733–741 (in Chinese with English abstract).
- Xiong Xiaolin, Zhao Zhenhua, Zhu Jinchu, Rao Bing and Lai Mingyuan, 1998. Partitioning of F between aqueous fluids and albite granite melt and its petrogenetic and metallogenic significance. *Chinese Journal of Geochemistry*, 17(4): 303–310.
- Xue Mingxuan, 2012. *Metallogenesis of endogenic gold deposits in Heilongjiang Province*. Changchun: Jilin University (Ph.D thesis): 1–176 (in Chinese with English abstract).
- Yang, H., Ge, W.C., Zhao, G.C., Yu, J.J., and Zhang, Y.L., 2015. Early Permian–Late Triassic granitic magmatism in the Jiamusi–Khanka Massif, eastern segment of the Central Asian Orogenic Belt and its implications. *Gondwana Research*, 27 (4): 1509–1533.
- Yang, J.H., Wu, F.Y., Wilde, S.A., and Zhao, G.C., 2008. Petrogenesis and geodynamics of Late Archean magmatism in eastern Hebei, eastern North China Craton: geochronological, geochemical and Nd–Hf isotopic evidence. *Precambrian Research*, 167(1–2): 125–149.
- Yuan, H.L., Gao, S., Liu, X.M., Li, H.M., Gunther, D., and Wu, F.Y., 2007. Accurate U–Pb age and trace element determinations of zircon by laser ablation–inductively coupled plasma mass spectrometry. *Geostandards and Geoanalytical Research*, 28(3): 353–370.
- Zeng Zhigang, Li Chaoyang, Liu Yuping and Tu Guangzhi, 1998. REE Geochemistry of scheelite of two genetic types from Nanyangtian, Southeastern Yunnan. *Geology Geochemistry*, 26 (2): 34–38 (in Chinese with English abstract).
- Zhang Hongfu, Menzies, M.A., Lu Fengxiang and Zhou Xinhua, 2000. Major and trace element studies on garnets from Palaeozoic kimberliteborne mantle xenoliths and megacrysts from the North China craton. *Science in China Series D* (Earth Sciences), 43(4): 423–430.
- Zhang Xingzhou, Ma Yuxia, Chi Xiaoguo, Zhang Fengxu, Sun Yuewu, Guo Ye and Zeng Zhen, 2012. Discussion on Phanerozoic tectonic evolution in Northeastern China. *Journal of Jilin University* (Earth Science Edition), 42(5): 1269–1285 (in Chinese with English abstract).
- Zhang Yuxue, Liu Yimao, Gao Sideng and He Qiguang, 1990.

- Earth elements geochemical characteristics of tungstenic minerals: A distinguishing sign for ore-forming type. *Chinese Journal of Geochemistry*, 9 (4): 11–20.
- Zhang Zhenjie, Cheng Qiuming, Yao Lingqing, Bai Huishan and Licheng, 2016. Zircon U-Pb-Hf isotopic systematics and geochemistry of the granites in the Wurinitu molybdenum deposit, Inner Mongolia, China: implications for tectonic setting and genetic type of mineralization. *Acta Geologica Sinica* (English Edition), 90(6): 2066–2079.
- Zhao Hualei, 2014. *Ore genesis and geodynamic settings of tungsten deposits in eastern Jilin and Heilongjiang Provinces*. Changchun: Jilin University (Ph.D thesis): 1–139 (in Chinese with English abstract).
- Zhao Hualei, Ren Yunsheng, Ju Nan, Wang Hui and Hou Kejun, 2011. Geochronology and geochemistry of metallogenic intrusion in Baishilazi tungsten deposit of eastern Yanbian area, Northeast China. *Journal of Jilin University* (Earth Science Edition), 41(6): 1726–1735 (in Chinese with English abstract).
- Zhao Liangliang, Wang Zongqi and Zhang Xingzhou, 2014. Detrital zircon U-Pb dating of Majiajie Group and its tectonic implications. *Acta Petrologica Sinica*, 30(6): 1769–1779 (in Chinese with English abstract).
- Zhou Jianbo, Zeng Weishun, Gao Jialin, Han Jie and Guo Xiaodan, 2012. The tectonic framework and evolution of the NE China: from ~500 Ma to ~180 Ma. *Journal of Jilin University* (Earth Science Edition), 42(5): 1298–1316 (in Chinese with English abstract).
- Zhou Jianbo, Zhang Xingzhou, Wilde, S.A. and Zheng Changqing, 2011. Confirming of the Heilongjiang ~500 Ma Pan-African khondalite belt and its tectonic implications. *Acta Petrologica Sinica*, 27(4): 1235–1245 (in Chinese with English abstract).
- Zhou, J.B., and Wilde, S.A., 2013. The crustal accretion history and tectonic evolution of the NE China segment of the Central Asian Orogenic Belt. *Gondwana Research*, 23 (4): 1365–1377.
- Zhou, J.B., Wilde, S.A., Zhang, X.Z., and Zheng, C.Q., 2011a. Early Paleozoic metamorphic rocks of the Erguna block in the Great Xing'an Range, NE China: Evidence for the timing of magmatic and metamorphic events and their tectonic implications. *Tectonophysics*, 499 (1–4): 105–117.
- Zhou, J.B., Wilde, S.A., Zhang, X.Z., Zhao, G.C., and Liu, F.L., 2011b. A >1300 km Late-African metamorphic belt in NE China: New evidence from the Xing'an Block and its tectonic implications. *Tectonophysics*, 509(3): 280–292.
- Zhou, J.B., Wilde, S.A., Zhang, X.Z., Zhao, G.C., Zheng, C.Q., Wang, Y.J., and Zhang, X.H., 2009. The onset of Pacific margin accretion in NE China: Evidence from the Heilongjiang high-pressure metamorphic belt. *Tectonophysics*, 478(3): 230–246.
- Zhou, J.B., Wilde, S.A., Zhao, G.C., Zhang, X.Z., Zheng, C.Q., Wang, H. and Zeng, W.S., 2010a. Pan-African metamorphic and magmatic rocks of the Khanka Massif, NE China: further evidence regarding their affinity. *Geological Magazine*, 147 (5): 737–749.
- Zhou, J.B., Wilde, S.A., Zhao, G.C., Zhang, X.Z., Zheng, C.Q., and Wang, H., 2010b. New SHRIMP U-Pb Zircon ages from the Heilongjiang complex in NE China: Constraints on the Mesozoic evolution of NE China. *American Journal of Science*, 310: 1024–1053.
- Zhou, J.B., Wilde, S.A., Zhao, G.C., Zhang, X.Z., Wang, H., and Zeng, W.S., 2010c. Was the easternmost segment of the Central Asian Orogenic Belt derived from Gondwana or Siberia: An intriguing dilemma? *Journal of Geodynamics*, 50 (3): 300–317.
- Zhu Decheng, Lü Dawei, Shen Xiaoli, Yang Qing, Li Dandan, Ren Tianlong and Yang Shipeng, 2016. Discovery and geological significance of Neoproterozoic metamorphic granite in Jimo, Shandong Province, eastern China. *Acta Geologica Sinica* (English Edition), 90(6): 2080–2096.
- Zhu Xinyou, Wang Jingbin, Wang Yanli and Chen Xiyin, 2015. The role of magma-hydrothermal transition fluid in the skarn-type tungsten mineralization process: A case study from the Shizhuyuan tungsten and tin polymetallic ore deposit. *Acta Petrologica Sinica*, 31(3): 891–905 (in Chinese with English abstract).

#### About the first author

HAO Yujie, male, born in 1987 in Jinzhong City, Shanxi Province; PhD; graduated from Jilin University; engineer of College of Earth Sciences, Jilin University; majoring in ore deposit research. Email: haoyujie@jlu.edu.cn.